TVD Fluxes for the High-Order ADER Schemes

E. F. Toro[1] and V. A. Titarev[2]

[1] Laboratory of Applied Mathematics, Faculty of Engineering, University of Trento, Trento, Italy, e-mail: Toro@ing.unitn.it, web page: http://www.ing.unitn.it/toro/

[2] Department of Mathematics, Faculty of Science, University of Trento, Trento, Italy, e-mail: Titarev@science.unitn.it, web page http://www.science.unitn.it/~titarev

Abstract

Within the class of high order schemes for hyperbolic conservation laws, those that make use of a first-order monotone flux as the building block, are amongst the most successful. Examples include TVD methods, ENO/WENO methods and ADER methods. In this paper we propose to use a TVD flux, instead of a first-order monotone flux, as the building block for designing high-order methods; we implement the ideas in the context of ADER schemes via a new flux expansion. Systematic assessment of the new schemes shows substantial gains in accuracy; these are particularly evident for problems involving long time evolution.

Key words: high-order schemes, ADER, essentially non-oscillatory, generalised Riemann problem, flux expansion, TVD flux, WAF flux.

1. Introduction

We are concerned with shock-capturing numerical schemes of high-order of accuracy for computing solutions to hyperbolic conservation laws. It is well known that reconciling high-order of accuracy and absence of unphysical oscillations in the vicinity of discontinuities, such as shocks, poses a serious challenge to the algorithm designer. In fact, Godunov [5] proved about half a century ago that linear methods that are free from spurious oscillations cannot be of accuracy greater than one. Much work has been done since then to circumvent Godunov's theorem, which involves the design of schemes that must necessarily be non-linear, even if applied to linear problems. Amongst successful developments in this direction we have TVD methods [8, 23, 44, 19, 14, 31], ENO and WENO methods [9, 15, 7, 1], and more recently, ADER methods [35, 38, 26, 40, 21, 24].

This paper is about the class of ADER schemes for computing solutions to hyperbolic conservation laws. ADER [35] is a Godunov-type approach that allows the construction of schemes of an arbitrary order of accuracy in both space and time [38, 26, 21, 24]. A precursor to ADER is the Modified GRP (MGRP) method [32], which in turn results from a simplification to the GRP (Generalised Riemann Problem) scheme [3], in which the initial data for the local Riemann problem consists of two piece-wise linear distributions. See the related works of Men'shov [18, 16, 17]. In the MGRP one replaces the difficulty of solving the generalised Riemann problem with piece-wise linear data with that of solving two conventional Riemann problems, namely a non-linear problem for the state variables and a linear Riemann problem for the gradients of the state variables. It appears as if it was Kolgan [11, 12, 13] who first proposed to generalise the Riemann problem from that with piece-wise constant data to that with piece-wise linear data, producing in this manner a Godunov-type scheme of second order spatial accuracy. This scheme is often referred to as the Godunov-Kolgan scheme. Spurious oscillations are controlled by applying Kolgan's principle of minimal values of derivatives. More well-known developments are due to van Leer [41, 42] and many others.

The ADER approach takes the Modified GRP approach (MGRP) a step further by considering a generalised Riemann problem with initial conditions consisting of two data states defined by two polynomial functions of arbitrary degree [38]. This generalised Riemann problem is solved in the same manner as for the MGRP scheme, that is one solves a non-linear Riemann problem for the state variables and $(m-1)$ linear Riemann problems for the derivatives of the state variables; here $(m-1)$ is the order of the polynomials and m is the order of accuracy in space and time of the resulting schemes.

For linear equations, the formulation of the ADER schemes goes through in two and three space dimensions [35]. Implementations of ADER schemes of up to 10^{th} order of accuracy in space and time in one and two space dimensions are reported in [35, 21]. Extension of the ADER approach to nonlinear systems relies on the solution of the relevant generalised Riemann problem reported in [38]. The solution procedure is also valid for systems containing source terms. Corresponding numerical schemes are reported in [25, 39, 26, 40, 24]. In addition to reaction terms, the ADER formalism extends directly to include diffusion terms, which, in a very natural way, enter the flux computation via the solution of an inhomogeneous generalised Riemann problem; see [25, 40, 29] for numerical implementations for the nonlinear scalar case. The ADER approach as outlined so far relies on a Taylor series expansion in time of the solution of the generalised Riemann problem as represented by a state vector. We call this *state-expansion* ADER.

In this paper we first present a new version of the ADER approach in which the Taylor expansion is performed in terms of the flux vector. We call the scheme *flux-expansion* ADER. We build the flux rather than the state expansion in time to achieve an arbitrary order of accuracy both in space and time. Different fluxes can then be used as the building block, such as upwind or centred monotone fluxes. Then, by re-interpreting the fully expanded ADER scheme for the model hyperbolic equation, we propose to use a TVD flux, instead of a first-order monotone flux, as the building block. Of the upwind TVD fluxes available we find that the Weighted Average Flux (WAF) [33, 34, 31] is the most easily applied. The WAF flux achieves second order in space and time without performing data reconstruction, that is, by solving the conventional Riemann problem associated with the first-order Godunov scheme. This feature of the WAF method makes it particularly suitable for use in the ADER flux expansion. The resulting schemes are superior to both the original ADER schemes and the original TVD WAF scheme. In particular, the 'squaring' effect of TVD schemes on smooth regions, when used with compressive flux limiters, is eliminated; in addition, we retain the desirable property of high resolution of discontinuities associated with linearly degenerate fields provided by TVD schemes with compressive limiters. These advantageous properties of the resulting ADER-WAF schemes do not depend on tuning parameters. Conventionally, the limiting case of no reconstruction of data (piece-wise constant data) leads to the basic first-order scheme associated with the first-order monotone flux used as the building block. For the schemes presented in this paper the limiting case of no data reconstruction produces a second-order TVD scheme.

We carry out a systematic assessment of the constructed numerical schemes. We do so for a set of carefully selected test problems, with particular emphasis on testing the accuracy of the schemes for *very long time evolution*, as it is long-time evolution for which the sophistication of high-order must be justified. We compare results against exact solutions and against reference solutions computed with very fine meshes. The new schemes are systematically compared with conventional TVD methods, such as the WAF method, and state-of-the art WENO and MPWENO schemes.

The rest of the paper is organised as follows. In Section 2 we review the state-expansion ADER approach. The flux-expansion ADER is described in Section 3. In Section 4 we briefly review the Weighted Average Flux (WAF) method. In Section 5 we introduce the WAF flux in the ADER flux expansion. Numerical results are given in Section 6. Conclusions are drawn in Section 7.

2. State-expansion ADER schemes

We consider hyperbolic systems in conservation form

$$\partial_t \mathbf{Q} + \partial_x \mathbf{F}(\mathbf{Q}) = \mathbf{0} \tag{1}$$

along with initial and boundary conditions. Here $\mathbf{Q}(x,t)$ is the vector of unknown conservative variables and $\mathbf{F}(\mathbf{Q})$ is the physical flux vector. Consider now a control volume in $x-t$ space $I_i \times [t^n, t^{n+1}]$ of dimensions $\Delta x = x_{i+1/2} - x_{i-1/2}$, $\Delta t = t^{n+1} - t^n$, where $I_i = [x_{i-1/2}, x_{i+1/2}]$. Integrating (1) on $I_i \times [t^n, t^{n+1}]$ we obtain

$$\mathbf{Q}_i^{n+1} = \mathbf{Q}_i^n - \frac{\Delta t}{\Delta x}\left(\mathbf{F}_{i+1/2} - \mathbf{F}_{i-1/2}\right), \tag{2}$$

where $\mathbf{Q}_i^n$ and $\mathbf{F}_{i+1/2}$ are given by

$$\mathbf{Q}_i^n = \frac{1}{\Delta x}\int_{x_{i-1/2}}^{x_{i+1/2}} \mathbf{Q}(x,t^n)\,dx\,, \quad \mathbf{F}_{i+1/2} = \frac{1}{\Delta t}\int_{t^n}^{t^{n+1}} \mathbf{F}(\mathbf{Q}(x_{i+1/2},t))\,dt. \tag{3}$$

For a given (arbitrary) order of accuracy m the numerical flux of the corresponding ADER scheme is computed in the following way. At each cell interface $x_{i+1/2}$ we pose the generalised Riemann problem (GRP_{m-1}) with initial condition consisting of two polynomials of order $(m-1)^{\text{th}}$, namely

$$\begin{aligned} &\text{PDE:} \qquad \partial_t \mathbf{Q} + \partial_x \mathbf{F}(\mathbf{Q}) = \mathbf{0} \\ &\text{IC:} \qquad \mathbf{Q}(x,0) = \begin{cases} \mathbf{Q}_L(x) = \mathbf{p}_i(x), & x < x_{i+1/2} \\ \mathbf{Q}_R(x) = \mathbf{p}_{i+1}(x), & x > x_{i+1/2} \end{cases} \end{aligned} \tag{4}$$

The polynomials $\mathbf{p}_i(x)$ represent reconstructed point-wise values of the solution in each cell. In all numerical examples given here we use WENO reconstruction in characteristic variables, in much the same way as in WENO schemes [9, 7, 22]. A WENO reconstruction polynomial is defined as a weighted combination of all polynomials from r stencils of the underlying r^{th} order ENO schemes. The nonlinear WENO weights are written as

$$\omega_k = \frac{\alpha_k}{\sum_{l=0}^{r-1}\alpha_l}, \quad \alpha_k = \frac{C_k}{(\varepsilon+\beta_k)^p}\,. \tag{5}$$

Here C_k are optimal weights for the linear scheme, ε is a small parameter to avoid division by zero; we set $\varepsilon = 10^{-20}$ for ADER schemes. The smoothness indicator β_k is designed in such a way as to be of order of unity when $\mathbf{Q}(x,t^n)$ is discontinuous in the k^{th} stencil and $\beta_k = O(h^2)$ when $\mathbf{Q}(x,t^n)$ is smooth. As a result the discontinuous stencils are assigned weights which are of order $O((\varepsilon+h^2)^p)$ and the reconstruction procedure emulates the ENO idea. An important issue is the choice of the parameter p. In general $p=2$ works well for WENO schemes with weighted piece-wise linear and piece-wise parabolic reconstruction. In the ADER approach, however, the nonlinear weights have to control possible oscillations in the derivatives which are of order of $O(h^{1-r})$ for the r^{th} order ADER scheme. Because of this we require that $2p+1-r$ be positive and large enough to suppress oscillations. We find that $p=2$ works well for third and forth order ADER schemes. However, for higher order we use larger values, e.g. $p=4$. Note that $p\to\infty$ leads to an ENO-type reconstruction; thus one should not use very large values of the parameter p.

According to the method developed in [38] the approximate solution $\mathbf{Q}(x_{i+1/2},\tau)$ of (4) is sought as a Taylor expansion in time for the interface state

$$\mathbf{Q}(x_{i+1/2},\tau) = \mathbf{Q}(x_{i+1/2},0+) + \sum_{k=1}^{m-1}\left[\partial_t^{(k)}\mathbf{Q}(x_{i+1/2},0+)\right]\frac{\tau^k}{k!}\,, \tag{6}$$

where

$$\partial_t^{(k)}\mathbf{Q}(x,t) = \frac{\partial^k}{\partial t^k}\mathbf{Q}(x,t), \quad 0+ \equiv \lim_{\tau\to 0+}\tau$$

The leading term $\mathbf{Q}(x_{i+1/2},0+)$ accounts for the interaction of the boundary extrapolated values $\mathbf{Q}_L(x_{i+1/2})$ and $\mathbf{Q}_R(x_{i+1/2})$ in (4) and is the Godunov state of the conventional nonlinear (piece-wise constant data) GRP_0

$$\left.\begin{array}{ll} \text{PDE:} & \partial_t \mathbf{Q} + \partial_x \mathbf{F}(\mathbf{Q}) = \mathbf{0} \\ \text{IC:} & \mathbf{Q}(x,0) = \left\{ \begin{array}{ll} \mathbf{Q}_L(x_{i+1/2}) & \text{if} \quad x < x_{i+1/2} \\ \mathbf{Q}_R(x_{i+1/2}) & \text{if} \quad x > x_{i+1/2} \end{array} \right. \end{array}\right\} \tag{7}$$

The Cauchy-Kowalewski procedure is then applied to replace all time derivatives in expansion (6) by space derivatives. A detailed description of this procedure for the Euler equations can be found in [9]. Using the algebraic manipulator MAPLE we have produced an optimised FORTRAN code implementing the Cauchy-Kowalewski procedure for the Euler equations. In this code time derivatives of the conservative variables are expressed in terms of their spatial derivatives. This MAPLE program is available from the authors on request.

An observation of key value for the ADER schemes is that the k^{th} spatial derivative of the solution $\mathbf{Q}^{(k)} \equiv \partial_x^{(k)} \mathbf{Q}$ obeys the following inhomogeneous evolution system:

$$\partial_t \mathbf{Q}^{(k)} + \mathbf{A}(\mathbf{Q}) \partial_x \mathbf{Q}^{(k)} = \mathbf{G}_k(\mathbf{Q}, \mathbf{Q}^{(1)}, \ldots, \mathbf{Q}^{(k-1)}), \tag{8}$$

where $\mathbf{A}$ is the Jacobian matrix of system (1). The equations (8) are obtained by manipulating derivatives of (4) and making use of the Cauchy-Kowalewski procedure. The right hand side $\mathbf{G}_k$ is an algebraic function of $\mathbf{Q}$ and its lower-order derivatives and vanishes when the governing system is linear with constant coefficients, that is when $\mathbf{A}$ is a constant matrix. As we only need $\mathbf{Q}^{(k)}$ at the first-instant interaction of left and right states (time approaches zero from above) we can neglect the effect of the source terms in (8). Thus, to find the relevant term in the expansion we solve the following *linearised conventional* Riemann problem

$$\left.\begin{array}{ll} \text{PDE:} & \partial_t \mathbf{Q}^{(k)} + \mathbf{A}^{(0)}_{i+1/2} \partial_x \mathbf{Q}^{(k)} = \mathbf{0}, \quad \mathbf{A}^{(0)}_{i+1/2} = \mathbf{A}(\mathbf{Q}(x_{i+1/2},0+)) \\ \text{IC:} & \mathbf{Q}^{(k)}(x,0) = \left\{ \begin{array}{ll} \partial_x^{(k)} \mathbf{Q}_L(x_{i+1/2}), & x < x_{i+1/2} \\ \partial_x^{(k)} \mathbf{Q}_R(x_{i+1/2}), & x > x_{i+1/2} \end{array} \right. \end{array}\right. \tag{9}$$

The vector-valued function $\mathbf{Q}^{(k)}(x/\tau)$ is a similarity solution of (9) and the relevant value at the interface is obtained by evaluation this vector at $(x - x_{i+1/2})/\tau = 0$; we call this value, the Godunov state. Note that the Jacobian matrix $\mathbf{A}^{(0)}_{i+1/2}$ is the same for all $\mathbf{Q}^{(k)}$ and is evaluated only once.

Finally, having evolved all space derivatives at the cell interface $x_{i+1/2}$ we form the Taylor expansion (6), which becomes:

$$\mathbf{Q}(x_{i+1/2},\tau) = \mathbf{b_0} + \mathbf{b_1}\tau + \mathbf{b_2}\tau^2 + \ldots, \mathbf{b_{m-1}}\tau^{m-1}, \quad 0 \le \tau \le \Delta t \tag{10}$$

and which approximates the interface state for $0 \le \tau \le \Delta t$ to m^{th} order of accuracy. Here the coefficients $\mathbf{b_k}$ are constant vectors, independent of time. Having obtained the solution of the generalised Riemann problem we now evaluate the intercell numerical flux, for which there are two options. The first one (reported in [26]) is to use an appropriate

Gaussian rule applied to the time integral in (3) with the intercell state $\mathbf{Q}(x_{i+1/2},\tau)$ given by (10):

$$\mathbf{F}_{i+1/2} = \sum_{\alpha=0}^{K_\alpha} \mathbf{F}(\mathbf{Q}(x_{i+1/2}, \gamma_\alpha \Delta t))\, \omega_\alpha, \tag{11}$$

where γ_j and ω_j are properly scaled nodes and weights of the rule and K_α is the number of nodes. The second option (new) is discussed in the next section.

3. Flux expansion in the ADER approach

The idea of the flux expansion in the ADER approach is the following. First we solve the generalised Riemann problem at the cell interface $x_{i+1/2}$ and obtain the approximate solution $\mathbf{Q}(x_{i+1/2},\tau)$ as given in (10). Next, instead of integrating this approximate solution as in (11) we seek the Taylor expansion of the flux in time at $x_{i+1/2}$, namely

$$\mathbf{F}(x_{i+1/2},\tau) = \mathbf{F}(x_{i+1/2},0+) + \sum_{k=1}^{m-1} \left[\partial_t^{(k)} \mathbf{F}(x_{i+1/2},0+)\right] \frac{\tau^k}{k!}. \tag{12}$$

From (3) and (12) the numerical flux is now given by

$$\mathbf{F}_{i+1/2} = \mathbf{F}(x_{i+1/2},0+) + \sum_{k=1}^{m-1} \left[\partial_t^{(k)} \mathbf{F}(x_{i+1/2},0+)\right] \frac{\Delta t^k}{(k+1)!}\,. \tag{13}$$

The leading term $\mathbf{F}(x_{i+1/2},0+)$ accounts for the first interaction of left and right boundary extrapolated values and is computed as a certain monotone flux of the GRP_0 (7). Use of the Godunov flux produces the scheme which has the same formal accuracy as the state-expansion approach. Of course, we can also take $\mathbf{F}(x_{i+1/2},0+) = \mathbf{F}(\mathbf{Q}(x_{i+1/2},0+))$ as well. However, we can improve upon this by using a higher order non-oscillatory flux. This will be discussed in Section 5.

Several options exist to evaluate the remaining higher order terms. In this paper we do it in the following way. We express time derivatives of the flux in (13) via time derivatives of the intercell state $\mathbf{Q}(x_{i+1/2},\tau)$. As an example, we consider here the particular case of the time-dependent, one dimensional compressible Euler equations for a polytropic gas:

$$\left.\begin{aligned} \partial_t \mathbf{Q} + \partial_x \mathbf{F}(\mathbf{Q}) &= \mathbf{0} \\ \mathbf{Q} &= (\rho, m, E)^T \\ \mathbf{F}(\mathbf{Q}) &= \mathbf{Q}u + (0, p, pu)^T \\ p &= (\gamma-1)(E - \tfrac{1}{2}\rho u^2) \end{aligned}\right\} \tag{14}$$

where ρ, u, p and E are density, velocity, pressure and total energy, respectively; $m = \rho u$ is momentum and γ is the ratio of specific heats. The time derivatives of the flux are expressed via time derivatives of the dependent variables as, for example,

$$\left.\begin{aligned} \partial_t \mathbf{F}(\mathbf{Q}) &= (m_t,\, m_t u + m u_t + p_t,\, u_t(E+p) + u(E_t + p_t))^T \\ \partial_t^{(2)} \mathbf{F}(\mathbf{Q}) &= (m_{tt},\, m_{tt}u + 2m_t u_t + m u_{tt} + p_{tt}, \\ &\qquad u_{tt}(E+p) + 2u_t(E_t+p_t) + u(E_{tt} + p_{tt}))^T \end{aligned}\right\} \tag{15}$$

It is obvious that this procedure can be carried out for any given order. Again, an algebraic manipulator can be used to produce the FORTRAN output. All terms on the right hand

side of (15) are the evolved values of conservative variables and their derivatives, see (10). No numerical quadrature is then required to compute the numerical flux.

Another way of evaluating higher order terms in the flux expansion (13) is to derive evolution equations for spatial derivatives of the flux and then substitute the time derivatives $\partial_t^{(k)}\mathbf{F}$ by spatial derivatives via the Cauchy-Kowalewski procedure. Again the state expansion must be carried out to compute all evolved time and spatial derivatives of the conservative variables. Results for fifth order ADER schemes using this approach applied to Burgers' equation can be found in [24]. They show that the derived schemes retain very high order of accuracy. A detailed evaluation of this variant for nonlinear systems will be reported elsewhere.

Both formulations of the ADER approach perform very satisfactorily as compared with state-of-art schemes such as the ENO/WENO schemes. However, as observed earlier, discontinuities associated with linearly degenerate fields, such as contact discontinuities and shear waves, are badly smeared *for very long time evolution* . In fact, this observation applies also to other very-high order methods such as ENO/WENO schemes. On the other hand, it is also known that some upwind TVD methods, e.g. the Weighted Average Flux (WAF) method [33, 34, 31], have the capability of providing much sharper resolution of this type of waves.

One of the motivations of this paper is to enhance the accuracy of the ADER schemes by making use of the WAF flux as part of the flux expansion of the solution of the generalised Riemann problem (4). That is, we propose to use a TVD flux rather than a first-order monotone flux as the building block of our high order methods. In the next section we first briefly review the WAF scheme for one-dimensional scalar and compressible Euler equations, as it will be the WAF flux that will be incorporated in the framework of ADER schemes in section 5.

4. Review of the WAF method

The Weighted Average Flux (WAF) method [33, 34, 31] defines an intercell flux as

$$\mathbf{F}_{i+1/2}^{WAF} = \frac{1}{t_2 - t_1}\frac{1}{x_2 - x_1}\int_{t_1}^{t_2}\int_{x_1}^{x_2} \mathbf{F}(\mathbf{Q}^*(x,t))\,dx\,dt\ . \tag{16}$$

A special case is the formula

$$\mathbf{F}_{i+1/2}^{WAF} = \frac{1}{\Delta x}\int_{-\Delta x/2}^{\Delta x/2} \mathbf{F}(\mathbf{Q}_{i+1/2}(x, t^n + \Delta t/2))\,dx\ . \tag{17}$$

Assuming further that $\mathbf{Q}_{i+1/2}$ is the solution of the conventional piece-wise constant Riemann problem (GRP_0) with initial data $\mathbf{Q}_i^n$ and $\mathbf{Q}_{i+1}^n$ we may write

$$\mathbf{F}_{i+1/2}^{WAF} = \frac{1}{2}(\mathbf{F}_i^n + \mathbf{F}_{i+1}^n) - \frac{1}{2}\sum_{k=1}^{N} c_k \Delta\mathbf{F}_{i+1/2}^{(k)}\ , \tag{18}$$

where $c_k = \frac{S_k \Delta t}{\Delta x}$ is the Courant number associated with wave k of speed S_k in the solution of the Riemann problem GRP_0. Flux (18) when used in (2) gives a second order accurate scheme in space and time. It is important to realise, at this stage, that such second-order accuracy is achieved without data reconstruction. This feature of the WAF method will make it particularly useful in the context of higher-order ADER schemes, see section 5.

Scheme (18) is linear and thus oscillatory. A non-oscillatory, TVD, version is given by

$$\mathbf{F}_{i+1/2}^{WAF} = \frac{1}{2}(\mathbf{F}_i^n + \mathbf{F}_{i+1}^n) - \frac{1}{2}\sum_{k=1}^{N} \text{sign}(c_k) A_k \Delta\mathbf{F}_{i+1/2}^{(k)}, \tag{19}$$

where A_k is a WAF flux limiter related to a conventional flux limiter B_k via

$$A_k = 1 - (1 - |c_k|)B_k. \tag{20}$$

The flux limiter $B_k(r)$ depends on a flow parameter $r^{(k)}$ which refers to wave k in the solution of the Riemann problem and is the following ratio

$$r^{(k)} = \begin{cases} \dfrac{\Delta q_{i-1/2}^{(k)}}{\Delta q_{i+1/2}^{(k)}}, & \text{if} \quad c_k > 0, \\ \\ \dfrac{\Delta q_{i+3/2}^{(k)}}{\Delta q_{i+1/2}^{(k)}}, & \text{if} \quad c_k < 0, \end{cases} \tag{21}$$

where q is a suitable variable depending on the problem being solved. This variable must change across each wave family in the solution of the Riemann problem; $\Delta q_{l+1/2}^{(k)}$ denotes the jump in q across wave k in the self-similar solution $\mathbf{Q}_{l+1/2}(\xi, \tau)$ in the Riemann problem with data $(\mathbf{Q}_l^n, \mathbf{Q}_{l+1}^n)$. For the Euler equations the choice $q = \rho$ (density) usually gives very satisfactory results.

The WAF method can be used with any Riemann solver available. It is recommended to use 'complete' Riemann solvers, that is those including all waves in their structure. We particularly recommend the HLLC Riemann solver [30, 36, 37], which is an improved variant of the HLL solver [10]. See also [2, 6]. An updated version of HLLC is found in [31]. For the 3D Euler equations

$$\mathbf{F}_{i+1/2}^{HLLC} = \begin{cases} \mathbf{F}_L, & \text{if} \quad 0 \le S_L, \\ \mathbf{F}_{*L} = \mathbf{F}_L + S_L(\mathbf{Q}_{*L} - \mathbf{Q}_L), & \text{if} \quad S_L \le 0 \le S_*, \\ \mathbf{F}_{*R} = \mathbf{F}_R + S_R(\mathbf{Q}_{*R} - \mathbf{Q}_R), & \text{if} \quad S_* \le 0 \le S_R, \\ \mathbf{F}_R, & \text{if} \quad 0 \ge S_R. \end{cases} \tag{22}$$

where for the WAF method (no reconstruction) $L = i$, $R = i + 1$ and

$$\mathbf{Q}_{*K} = \rho_K \left(\frac{S_K - u_K}{S_K - S_*}\right) \begin{bmatrix} 1 \\ S_* \\ v_K \\ w_K \\ \dfrac{E_K}{\rho_K} + (S_* - u_K)[S_* + \dfrac{p_K}{\rho_K(S_K - u_K)}] \end{bmatrix} \tag{23}$$

for $K = L$ and $K = R$. The wave speeds S_L, S_* and S_R must be estimated. We use the pressure-velocity estimates of Sect. 10.5.2 of [31].

Another possible version of WAF is obtained if one first defines a weighted average state as

$$\mathbf{Q}_{i+1/2}^{WAF} = \frac{1}{2}(\mathbf{Q}_i + \mathbf{Q}_{i+1}) - \frac{1}{2}\sum_{k=1}^{N} c_k \Delta \mathbf{Q}_{i+1/2}^{(k)}, \tag{24}$$

with a corresponding TVD version analogous to (19). The intercell flux is then

$$\mathbf{F}_{i+1/2} = \mathbf{F}(\mathbf{Q}_{i+1/2}^{WAF}). \tag{25}$$

Computationally, this state-average scheme is more efficient than (19) because it involves only one evaluation of the flux. For linear systems with constant coefficients (18) and (24)-(25) are equivalent. However, for the nonlinear systems, such as the Euler equations of gas dynamics, they are not and we recommend using the flux averaging (19) rather than state averaging.

5. TVD fluxes in the ADER approach

Consider the scalar linear advection equation:

$$\begin{aligned} \text{PDE:} \quad & \partial_t q + \partial_x f(q) = 0, \quad f = \lambda q, \quad \lambda = \text{const} \\ \text{IC:} \quad & q(x,0) = q_0(x) \end{aligned} \tag{26}$$

The scheme is now written as

$$q_i^{n+1} = q_i^n - \frac{\Delta t}{\Delta x}\left(f_{i+1/2} - f_{i-1/2}\right) \tag{27}$$

with flux expansion in time as

$$f(x_{i+1/2},\tau) = f(x_{i+1/2},0+) + \sum_{k=1}^{m-1}\left[\partial_t^{(k)} f(x_{i+1/2},0+)\right]\frac{\tau^k}{k!} \tag{28}$$

We note that since $f = \lambda q$ the state-expansion and flux-expansion schemes are identical; we have

$$\partial_t^{(k)} f(x,t) = (-\lambda)^k \partial_x^{(k)} f(x,t) \tag{29}$$

and the numerical flux has a closed form expression given by

$$f_{i+1/2} = f(x_{i+1/2},0+) + \sum_{k=1}^{m-1}\left[\partial_x^{(k)} f(x_{i+1/2},0+)\right]\frac{(-\lambda\Delta t)^k}{(k+1)!}. \tag{30}$$

The flux f and its spatial derivatives $\partial_x^{(k)} f = f^{(k)}$, $k = 0,\ldots,m-1$ satisfy the same advection equation as the unknown variable:

$$\left.\begin{aligned} \text{PDE:} \quad & \partial_t f^{(k)} + \lambda \partial_x f^{(k)} = 0 \\ \text{IC:} \quad & f(x,0) = \begin{cases} f_L^{(k)} = \lambda \partial_x^{(k)} q_L(x_{i+1/2}) & \text{if} \quad x < x_{i+1/2} \\ f_R^{(k)} = \lambda \partial_x^{(k)} q_R(x_{i+1/2}) & \text{if} \quad x > x_{i+1/2} \end{cases} \end{aligned}\right\} \tag{31}$$

On the other hand, they can be computed as fluxes from the Riemann problems for $q^{(k)} = \partial_x^{(k)} q(x,t)$:

$$\left.\begin{aligned} \text{PDE:} \quad & \partial_t q^{(k)} + \lambda \partial_x q^{(k)} = 0 \\ \text{IC:} \quad & q(x,0) = \begin{cases} q_L^{(k)} = \partial_x^k q_L(x_{i+1/2}) & \text{if} \quad x < x_{i+1/2} \\ q_R^{(k)} = \partial_x^k q_R(x_{i+1/2}) & \text{if} \quad x > x_{i+1/2} \end{cases} \end{aligned}\right\} \tag{32}$$

Substitution of the numerical flux into (27) gives the sought solution at time level $(n+1)$ and the full scheme may be written as

$$\left.\begin{aligned} q_i^{n+1} = q_i^n \quad & - \frac{(\Delta t)_0}{\Delta x}\left(\lambda p_{i+1/2}^{(0)} - \lambda p_{i-1/2}^{(0)}\right) \\ & - \frac{(\Delta t)_1}{\Delta x}\left(\lambda p_{i+1/2}^{(1)} - \lambda p_{i-1/2}^{(1)}\right) \\ & \cdots \\ & - \frac{(\Delta t)_k}{\Delta x}\left(\lambda p_{i+1/2}^{(k)} - \lambda p_{i-1/2}^{(k)}\right) \\ & \cdots \\ & - \frac{(\Delta t)_{m-1}}{\Delta x}\left(\lambda p_{i+1/2}^{(m-1)} - \lambda p_{i-1/2}^{(m-1)}\right) \end{aligned}\right\} \tag{33}$$

with

$$p_{i+1/2}^{(k)} = (-\lambda)^k q_{i+1/2}^{(k)}, \quad (\Delta t)_k = \frac{(\Delta t)^{k+1}}{(k+1)!}. \tag{34}$$

The first line of (33) is the Godunov first order upwind method applied to the state variable $q = \partial_x^{(0)} q$, if piece-wise constant reconstruction is used. The second line could be interpreted as solving an equation for the evolution of gradients $q^{(1)} = \partial_x^{(1)} q$, also using the Godunov first order upwind method. Similar interpretations apply to the remaining lines of (33).

Now the idea is to substitute the use of the Godunov first order upwind flux by some high order but non-oscillatory flux such as a flux of a Total Variation Diminishing (TVD) method. Such procedure could be applied at least to the first line of (33) Also, it seems to be beneficial to apply the procedure to all terms in the expansion.

Of the upwind TVD fluxes available it seems as if the flux-limited WAF method is the most suitable. Most of the modern TVD fluxes achieve non-oscillatory behaviour by applying a certain monotonicity constraint on the boundary extrapolated values. Thus, they cannot be used with the ADER approach because the application of such a constraint to boundary extrapolated values $\mathbf{Q}_R(x_{i+1/2})$ and $\mathbf{Q}_L(x_{i+1/2})$ would conflict with the sought order of accuracy of the ADER scheme. To our knowledge the only upwind second order TVD flux which does not need any constrains on $\mathbf{Q}_R(x_{i+1/2})$ and $\mathbf{Q}_L(x_{i+1/2})$ is the WAF flux, described in the previous section. We note that for the m^{th} order ADER scheme with WENO reconstruction we have $\mathbf{Q}_R(x_{i+1/2}) - \mathbf{Q}_L(x_{i+1/2}) = O(\Delta x^{2m-1})$ whenever the solution is smooth, and thus taking a weighted average of the solution of the generalised Riemann problem with data $\mathbf{Q}_R(x_{i+1/2})$ and $\mathbf{Q}_L(x_{i+1/2})$ does not change the formal order of accuracy.

The ADER-WAF schemes are obtained by using the WAF flux for the solution of (31) or WAF state in (32) with a TVD limiter. The numerical flux of the scheme can be evaluated either as the integral of the state expansion or the integral of the flux expansion at the cell interface.

The flow parameter for the k^{th} Riemann problem (including $k = 0$) is computed as

$$r = \begin{cases} \dfrac{q^{(k)}_{R,i-1/2} - q^{(k)}_{L,i-1/2}}{q^{(k)}_{R,i+1/2} - q^{(k)}_{L,i+1/2}}, & \text{if} \quad c > 0 \\ \\ \dfrac{q^{(k)}_{R,i+3/2} - q^{(k)}_{L,i+3/2}}{q^{(k)}_{R,i+1/2} - q^{(k)}_{L,i+1/2}}, & \text{if} \quad c < 0 \end{cases} \tag{35}$$

where $c = \frac{\lambda \Delta t}{\Delta x}$ is the Courant number.

The computation of the ratio r in (35) requires special attention when the denominator D is small, $|D| \leq \varepsilon$, say, where ε is a small positive number. For TVD methods, experience shows that the robustness of the methods does not depend too crucially on the way this step is handled, while accuracy does. The following two procedures are usually applied:

$$r = \frac{N}{D + \varepsilon} \tag{36}$$

$$r = \frac{\hat{N}}{\hat{D}}, \quad \hat{X} = \begin{cases} \varepsilon \, \text{sign}(1, X), & if \quad |X| \leq \varepsilon, \\ X, & \text{otherwise.} \end{cases} \tag{37}$$

Procedure (37) leads to more accurate results and it can be easily seen that for nearly uniform flow $r \approx 1$, leading to second order accuracy, the correct behaviour of a TVD scheme. This is not the case with procedure (36), which results in larger artificial diffusion. There is a third procedure given by

$$r = \begin{cases} \dfrac{N}{D}, & if \quad |D| \geq \varepsilon, \\ 0\,, & \text{otherwise.} \end{cases} \tag{38}$$

For the computations reported in this paper, procedure (37) was used successfully, except for a particular case, namely the linear advection equation for the forth order ADER-WAF scheme, for the second test problem and for the longest evolution time $t = 2000$. For such case procedure (38) was applied with satisfactory results. It seems to us as if the implementation of TVD criteria in the context of this paper, namely the construction of very high-order methods, may require some further investigations.

We find that the resulting ADER-WAF schemes show a very marked improvement in overall accuracy, particularly for *very long time evolution* (hundreds of thousands of time steps) of both smooth and non-smooth features. The performance, though, does depend on the particular choice of flux limiters but in general compressive limiters, such as the SUPERBEE limiter of Roe [19], give the best results. Isolated discontinuities associated with linearly degenerate fields are propagated indefinitely without smearing and the squaring effect of compressive limiters when used in conjunction with TVD methods is removed by the higher order terms in the flux expansion.

Now we turn to the nonlinear system case. In the expression for the numerical flux (13) we evaluate the leading term $\mathbf{F}(x_{i+1/2}, 0+)$ as the WAF flux with the HLLC Riemann solver. When the solution contains strong shocks we find it beneficial to use characteristic projections of the fluxes when applying TVD constraints in the following manner. Let $\mathbf{R}^{(0)}_{i+1/2}$ be a matrix whose columns are the right eigenvectors of the local Jacobian matrix

$\mathbf{A}^{(0)}_{i+1/2}$, defined in (9), and $\mathbf{L}^{(0)}_{i+1/2} = (\mathbf{R}^{(0)}_{i+1/2})^{-1}$ be a matrix whose rows are left eigenvectors of $\mathbf{A}^{(0)}_{i+1/2}$. These constant matrices of eigenvectors will be later utilised in the solution of the derivative Riemann problems. The projected values of the fluxes are then given by

$$\tilde{\mathbf{F}}^{(k)}_{i+1/2} = \mathbf{L}^{(0)}_{i+1/2} \mathbf{F}^{(k)}_{i+1/2} \tag{39}$$

where k denotes the wave k in the Riemann problem solution and should not be confused with the spatial derivative of order k. We evaluate the flux in terms of projected values

$$\tilde{\mathbf{F}}^{WAF}_{i+1/2} = \frac{1}{2}(\tilde{\mathbf{F}}_L + \tilde{\mathbf{F}}_R) - \frac{1}{2}\sum_{k=1}^{N} \mathrm{sign}(c_k) A_k \Delta \tilde{\mathbf{F}}^{(k)}_{i+1/2} \, . \tag{40}$$

The flow parameter r for the TVD limiter is given by (21). Finally, the leading term of the flux expansion is computed as the back projection:

$$\mathbf{F}(x_{i+1/2}, 0+) = \mathbf{F}^{WAF}_{i+1/2} = \mathbf{R}^{(0)}_{i+1/2} \tilde{\mathbf{F}}^{WAF}_{i+1/2} \, . \tag{41}$$

As to the remaining terms in the flux expansion they are evaluated as described in Section 3. The spatial derivatives $\mathbf{Q}^{(k)}(x_{i+1/2}, 0)$ are computed as the WAF state of the linear derivative Riemann problems (9), see (24), limited as in (19). As the flow parameter for the TVD limiter we use the first component of $\mathbf{Q}^{(k)}$, that is the k^{th} spatial derivative of density. The evaluation of the higher order terms is complete after we carry out the Cauchy-Kowalewski procedure. The flux is then given by (13).

6. Numerical results

In this section we show numerical results for the original ADER schemes [35, 26] and the new ADER-WAF schemes introduced in this paper. We compare the results of these schemes with those of other state-of-the art high order shock-capturing methods, such as WENO5 [7] and MPWENO9 [1], and also with conventional TVD schemes, such as WAF [33, 34, 31]. Here we use the finite-volume versions of WENO5 and MPWENO9 methods with third order TVD Runge-Kutta time stepping; we do so because we are computing discontinuous solutions and this rules out the use of higher order *linear* Runge-Kutta time discretisation methods used in [1]. For these schemes we set $\varepsilon = 10^{-6}$ in the WENO weights (5), as suggested in the original papers.

The linear stability condition for the WAF, WENO5, ADER and new ADER-WAF schemes is CFL ≤ 1, where CFL is the maximum Courant number for each time step; we use CFL=0.95 for these schemes. The monotonicity-preserving constraint used in the MPWENO9 scheme requires that CFL be lower than 0.33. In some cases, however, especially when the discontinuities are weak, larger CFL numbers might be used without introducing oscillations; such choice of the CFL numbers is problem-dependent and cannot be made in advance in practical calculations. On the other hand, lower CFL numbers allow the scheme to achieve higher convergence rate for smooth solutions. To be consistent, we set CFL=0.3 in all calculations made with the MPWENO9 scheme. Note that the WENO5, ADER3 and ADER3-WAF all use the same 5-point cell stencil; MPWENO9, ADER5 and ADER5-WAF use the larger 9-point cell stencil.

An important issue is the choice of test problems. We would like to emphasise here the importance of using *really* long time evolution problems, involving hundreds of thousands time steps, with solutions consisting of both discontinuities and smooth parts.

6.1 Scalar linear advection

Example 1. First we check the convergence properties of the new schemes. We solve the linear advection equation

$$\partial_t q + \partial_x q = 0 \tag{42}$$

with the initial conditions

$$q(x,0) = \sin(\pi x) \tag{43}$$

and

$$q(x,0) = \sin^4(\pi x) \tag{44}$$

defined on [-1,1]. Periodic boundary conditions are used. The error of cell averages is measured at the output time $t = 1$. Tables 1 and 2 show convergence rates and errors in different norms. We observe that all ADER and ADER-WAF schemes reach the designed order of accuracy. The size of errors shows that use of the TVD flux with the SUPERBEE limiter does not affect the formal accuracy of the ADER-WAF schemes. As expected, the errors of WENO5 and MPWENO9 schemes decrease with third order only. We note that our results for the MPWENO9 scheme differ from those of [1] because we use the third order TVD Runge-Kutta scheme, whereas in [1] a *linear* 9^{th} order Runge-Kutta method is used. However, as in [1], MPWENO9 is more accurate than the WENO5 scheme by a factor of ten for the CFL numbers used. Thus, increased order of spatial discretisation coupled with the smaller Courant number does improve the accuracy of this scheme. We observe that third order ADER schemes are more accurate than the WENO5 scheme and comparable with the MPWENO9 scheme, whereas both fifth order ADER schemes converge much faster than the WENO5 and MPWENO9 schemes. As expected, all higher order schemes outperform the second order WAF scheme when the mesh is refined. We note, however, that for initial condition (44) the WAF competes well with the WENO5 scheme up to a rather fine mesh of 80 cells. We also found that for this initial condition the accuracy of the WENO5 scheme is not sensitive to the choice of the CFL number and does not improve when the CFL number is decreased.

Example 2. Now we solve the model equation (42) for the following initial condition [7, 22, 1].

$$q(x,0) = \begin{cases} \exp\left(\ln 2\,(x+0.7)^2/0.0009\right), & -0.8 \le x \le -0.6 \\ 1, & -0.4 \le x \le -0.2 \\ 1 - |10x - 1|, & 0.0 \le x \le 0.2 \\ (1 - 100(x-0.5)^2)^{1/2}, & 0.4 \le x \le 0.6 \\ 0, & \text{otherwise} \end{cases} \tag{45}$$

This initial condition consists of a discontinuous square pulse and several continuous but narrow profiles. We use a baseline mesh of 200 cells and periodic boundary conditions. We compute the numerical solution at output times $t = 20$ and $t = 2000$. Note that for the last output time the initial profile is propagated 1000 times over the spatial domain. When CFL number of unity is used, this output time corresponds to 2×10^5 time steps. Results are shown in Figs. 1-8. In all figures the continuous line corresponds to the exact solution and symbols correspond to the numerical solution.

Figs. 1 and 2 show the results of the WAF scheme with the van Leer and SUPERBEE limiters. The numerical solution obtained with the van Leer limiter is acceptable for

Table 1: Convergence study for various schemes as applied to the model equation (42) with initial condition (43) at output time $t = 1$. Schemes WAF, WENO5, ADER and ADER-WAF used with CFL=0.95 and MPWENO9 used with CFL=0.3

Method	N	L_∞ error	L_∞ order	L_1 error	L_1 order
WAF	10	2.93×10^{-2}		1.88×10^{-2}	
van Leer	20	1.30×10^{-2}	1.18	8.62×10^{-3}	1.12
limiter	40	4.70×10^{-3}	1.46	1.53×10^{-3}	2.49
	80	1.93×10^{-3}	1.28	4.17×10^{-4}	1.88
	160	7.76×10^{-4}	1.31	1.01×10^{-4}	2.04
WENO5	10	5.05×10^{-2}		5.99×10^{-2}	
	20	4.51×10^{-3}	3.48	5.52×10^{-3}	3.44
	40	4.66×10^{-4}	3.28	5.95×10^{-4}	3.21
	80	5.51×10^{-5}	3.08	7.04×10^{-5}	3.08
	160	6.80×10^{-6}	3.02	8.68×10^{-6}	3.02
MPWENO9	10	1.22×10^{-3}		1.45×10^{-3}	
	20	1.07×10^{-4}	3.50	1.38×10^{-4}	3.39
	40	1.36×10^{-5}	2.98	1.73×10^{-5}	3.00
	80	1.71×10^{-6}	2.99	2.17×10^{-6}	2.99
	160	2.14×10^{-7}	3.00	2.72×10^{-7}	3.00
ADER3	10	4.62×10^{-3}		3.92×10^{-3}	
	20	2.05×10^{-4}	4.50	1.97×10^{-4}	4.32
	40	1.95×10^{-5}	3.40	2.06×10^{-5}	3.25
	80	2.29×10^{-6}	3.09	2.79×10^{-6}	2.89
	160	2.82×10^{-7}	3.02	3.56×10^{-7}	2.97
ADER5	10	1.14×10^{-4}		1.45×10^{-4}	
	20	7.66×10^{-7}	7.21	7.84×10^{-7}	7.53
	40	1.98×10^{-8}	5.27	2.52×10^{-8}	4.96
	80	6.07×10^{-10}	5.03	7.73×10^{-10}	5.03
	160	1.84×10^{-11}	5.05	2.34×10^{-11}	5.05
ADER3-WAF	10	2.64×10^{-3}		2.65×10^{-3}	
	20	2.44×10^{-4}	3.44	1.62×10^{-4}	4.04
	40	2.23×10^{-5}	3.45	1.38×10^{-5}	3.55
	80	2.36×10^{-6}	3.24	1.55×10^{-6}	3.16
	160	3.04×10^{-7}	2.95	1.89×10^{-7}	3.04
ADER5-WAF	10	1.32×10^{-4}		1.46×10^{-4}	
	20	1.41×10^{-6}	6.56	1.49×10^{-6}	6.61
	40	5.24×10^{-8}	4.75	4.53×10^{-8}	5.04
	80	1.44×10^{-9}	5.18	1.24×10^{-9}	5.19
	160	4.40×10^{-11}	5.04	4.46×10^{-11}	4.80

Table 2: Convergence study for various schemes as applied to the model equation (42) with initial condition (44) at output time $t = 1$. Schemes WAF, WENO5, ADER and ADER-WAF used with CFL=0.95 and MPWENO9 used with CFL=0.3

Method	N	L_∞ error	L_∞ order	L_1 error	L_1 order
WAF	10	1.36×10^{-1}		1.09×10^{-1}	
van Leer	20	4.74×10^{-2}	1.52	3.46×10^{-2}	1.66
limiter	40	1.84×10^{-2}	1.36	6.73×10^{-3}	2.36
	80	7.67×10^{-3}	1.26	1.92×10^{-3}	1.81
	160	3.10×10^{-3}	1.31	4.84×10^{-4}	1.99
WENO5	10	4.15×10^{-1}		3.68×10^{-1}	
	20	1.22×10^{-1}	1.76	1.20×10^{-1}	1.61
	40	2.42×10^{-2}	2.34	2.15×10^{-2}	2.48
	80	2.49×10^{-3}	3.28	2.34×10^{-3}	3.20
	160	2.81×10^{-4}	3.14	2.78×10^{-4}	3.08
MPWENO9	10	1.87×10^{-1}		1.50×10^{-1}	
	20	2.48×10^{-2}	2.92	2.45×10^{-2}	2.61
	40	1.82×10^{-3}	3.77	1.30×10^{-3}	4.24
	80	1.92×10^{-4}	3.24	1.11×10^{-4}	3.55
	160	2.81×10^{-5}	2.77	1.14×10^{-5}	3.28
ADER3	10	1.13×10^{-1}		9.02×10^{-2}	
	20	1.79×10^{-2}	2.66	1.25×10^{-2}	2.85
	40	1.77×10^{-3}	3.34	1.47×10^{-3}	3.09
	80	3.11×10^{-4}	2.51	1.35×10^{-4}	3.44
	160	3.97×10^{-5}	2.97	1.42×10^{-5}	3.25
ADER5	10	7.50×10^{-2}		6.17×10^{-2}	
	20	2.73×10^{-3}	4.78	2.84×10^{-3}	4.44
	40	4.95×10^{-4}	2.46	1.35×10^{-4}	4.40
	80	3.27×10^{-6}	7.24	1.02×10^{-6}	7.04
	160	2.63×10^{-8}	6.96	1.32×10^{-8}	6.27
ADER3-WAF	10	1.08×10^{-1}		9.21×10^{-2}	
	20	9.89×10^{-3}	3.45	8.17×10^{-3}	3.50
	40	1.48×10^{-3}	2.74	1.22×10^{-3}	2.75
	80	3.50×10^{-4}	2.08	1.20×10^{-4}	3.34
	160	4.38×10^{-5}	3.00	9.97×10^{-6}	3.59
ADER5-WAF	10	7.35×10^{-2}		6.01×10^{-2}	
	20	2.61×10^{-3}	4.82	2.29×10^{-3}	4.71
	40	4.29×10^{-4}	2.61	1.29×10^{-4}	4.15
	80	2.54×10^{-6}	7.40	1.09×10^{-6}	6.90
	160	3.19×10^{-8}	6.31	1.92×10^{-8}	5.82

$t = 20$ but unacceptable for $t = 2000$, since it does not contain any of the features present in the exact solution. When the SUPERBEE limiter is used the accuracy of the scheme is much higher (Fig. 2). In particular, we observe that the square pulse is well represented for all output times with almost the same number of cells across its two discontinuities. However, the semi-circular profile is 'squared' by the scheme. We remark that the error persists when the mesh is refined. This behaviour of TVD schemes associated with overcompressive limiters is well known.

Figs. 3 and 4 show results of the WENO5 scheme and the original ADER3 scheme. We observe that for the Courant number used the numerical solution obtained by the WENO5 scheme contains over and undershoots. These are significantly reduced when the Courant number is decreased three times; mesh refinement does not help. The numerical solution obtained by the ADER3 scheme is quite accurate for $t = 20$ but becomes unacceptable for $t = 2000$ (Fig. 4); the oscillations should be attributed to the *essentially* non-oscillatory nature of the scheme. It is likely that the small oscillations at the level of truncation error admitted at every time step have accumulated.

A surprising observation is that for the given mesh the overall accuracy of the WENO5 and ADER3 schemes is essentially the same as that of WAF with the van Leer limiter and much worse than that of WAF with the SUPERBEE limiter. It is commonly believed that higher order schemes produce better results for long time evolution problems. However, in this special case, a good second order (only first order in L_∞ norm) TVD scheme is more accurate than the WENO5 and ADER3 schemes; compare Fig. 2 with Figs. 3 and 4. Both the WENO5 and ADER3 smear the square pulse into a smooth Gaussian-like wave as much as the WAF scheme with the more diffusive van Leer limiter.

Fig. 5 shows results of the MPWENO9 scheme. We observe that this scheme is considerably more accurate than the WENO5 and ADER3 schemes, especially for the larger output time $t = 2000$. The numerical solution has all features of different shapes; note that the solution is fairly symmetric. This result is in line with the observations made by Balsara and Shu [1] that increasing the order of spatial discretisation can improve the quality of results even though the formal accuracy of the scheme remains that of the ODE solver, namely third order in the present computation. It is apparent, however, that even the scheme with such a high order of spatial discretisation cannot accurately compute contact discontinuities for long time evolution. We see that the square pulse has lost its top value and the two discontinuities are smeared to such an extent that at $t = 2000$ the square pulse resembles the semicircular profile. We conclude that all very-high order schemes considered so far, cannot resolve contact discontinuities as well as a conventional *second order* TVD scheme with a compressive limiter, such as the TVD WAF scheme with the more compressive SUPERBEE limiter.

Figs. 6 - 8 show results of the new ADER-WAF schemes of different orders. We observe that these schemes are superior to other schemes for all output times. The most obvious improvement over other methods is in the resolution of the square pulse; third and forth order schemes (Figs. 6 and 7) do not smear it as time evolves. We would like to stress that each discontinuity has five cells across it for *all output times*, that is, once the initial smearing of the discontinuity has been established it is propagated as a steady profile with a constant number of cells across it. Thus, ADER-WAF schemes combine the excellent resolution of contact discontinuities, typical of the WAF scheme with the SUPERBEE limiter, and higher order of accuracy in smooth regions, without the typical 'squaring' effect of TVD schemes with compressive limiters. We note that the ADER5-

WAF scheme does smear the square pulse for longer times. This is again expected since the higher order terms in the flux expansion weaken the effect of the compressive limiter. We also observe improvements in accuracy in the other parts of the solution when we move from the third to the fifth order scheme. The results of the ADER6-WAF scheme are only slightly better than those of ADER5-WAF and thus are omitted.

The importance of using very large output times and solutions containing both smooth and non-smooth features is quite clear here. Although higher order methods usually outperform conventional TVD schemes in convergence studies for short and moderate output times and very smooth solutions, TVD schemes are much faster and simpler and thus the difference in accuracy can be compensated by the use of a finer mesh. We observe that for the output time $t = 20$ most of the schemes give acceptable results. It is only the larger times which show the real difference in accuracy between different methods.

Table 3 shows a convergence study for different schemes at $t = 2000$. We present the errors of cell averages of the solution in the L_1 norm; in this norm all schemes should converge with the first order of accuracy. We observe that the WAF scheme with the SUPERBEE limiter converges very slowly when the mesh is refined. This is again expected due to the use of the SUPERBEE limiter. The WAF scheme with the van Leer limiter and the WENO5 scheme converge with the same speed and have virtually the same accuracy. However, the error of WENO5 for the mesh of 800 cells is still larger than that of the WAF scheme with the SUPERBEE limiter on the mesh of 200 cells. The WENO5 scheme is also oscillatory for the given Courant number. We note that when CFL=0.3 is used the numerical convergence rate of WENO5 is much worse but the scheme becomes monotone. The MPWENO9 scheme is far superior to the WENO5 scheme and converges with the expected first order (for cell averages). From the results of Table 3 the most accurate schemes are the ADER-WAF schemes. This is apparently due to the excellent resolution of the square pulse which is resolved very satisfactorily by these schemes. On the finest mesh of 1600 cells ADER3-WAF is more than 10 times more accurate than the WAF and WENO5 schemes and around 3 times more accurate than the MPWENO9 scheme. The ADER4-WAF scheme is in turn more accurate than the ADER3-WAF scheme by a factor of two for all meshes. The convergence rates of the ADER3-WAF and ADER4-WAF schemes actually exceed the theoretically expected rate of one (for cell averages). Figs. 9 and 10 show numerical results of ADER3-WAF and MPWENO9 schemes for meshes containing 400 and 1600 cells. We see that on the finest mesh the ADER3-WAF scheme seems to have converged to the exact solution, whereas the MPWENO9 scheme still shows significant smearing of the square pulse. These results are in line with Table 3. We note that on a personal computer for one-dimensional linear scalar advection MPWENO9 is around 5 times slower than ADER3-WAF and 3.5 times than ADER4-WAF when ran with the same CFL number. This is due to the fact that reconstruction step in the MPWENO9 scheme involves calculation of complicated and expensive smoothness indicators and has to be done *three* times for the third order Runge-Kutta time stepping. On top of this difference in efficiency one has to add a factor of three due to the smaller CFL numbers used in the MPWENO9 scheme, namely CFL=0.3 instead of CFL=0.95 for ADER-WAF schemes. This leads us to believe that for the one-dimensional linear scalar advection equation the finite-volume ADER-WAF schemes are superior to finite-volume version of WENO/MPWENO schemes for long time evolution problems.

Table 3: Convergence study for various schemes (for cell averages) as applied to the model equation (42) with initial condition (45) at output time $t = 2000$. Schemes WAF, WENO5, ADER and ADER-WAF used with CFL=0.95 and MPWENO9 used with CFL=0.3

	WAF, van Leer		WAF, SUPERBEE		WENO5	
N	L_1	r_1	L_1	r_1	L_1	r_1
200	5.52×10^{-1}		9.86×10^{-2}		5.62×10^{-1}	
400	3.47×10^{-1}	0.67	8.38×10^{-2}	0.24	3.25×10^{-1}	0.79
800	1.87×10^{-1}	0.90	8.05×10^{-2}	0.06	1.92×10^{-1}	0.76
1600	9.85×10^{-2}	0.92	8.03×10^{-2}	0.00	9.63×10^{-2}	0.99

	MPWENO9		ADER3-WAF		ADER4-WAF	
N	L_1	r_1	L_1	r_1	L_1	r_1
200	2.52×10^{-1}		1.54×10^{-1}		7.00×10^{-2}	
400	1.01×10^{-1}	1.31	5.95×10^{-2}	1.37	2.95×10^{-2}	1.24
800	4.95×10^{-2}	1.04	2.46×10^{-2}	1.27	1.11×10^{-2}	1.42
1600	2.40×10^{-2}	1.04	8.92×10^{-3}	1.46	4.54×10^{-3}	1.29

6.2 Euler equations of gas dynamics

We now assess the performance of different schemes for the one-dimensional Euler equations for a γ-law gas (14), with $\gamma = 1.4$ in all the results shown here. For WAF and ADER-WAF schemes we use the HLLC Riemann solver of Section 4. For WENO and MPWENO schemes we use the adaptive approximate-state Riemann solver described in Chapter 9 of [31]. This solver utilises a combination of the linearised Riemann solver, two-rarefaction Riemann solver and two-shock Riemann solver. We note that usually WENO schemes use Rusanov-type fluxes [20] as the building block for higher accuracy, see [15, 7, 1]. However, the use of an upwind flux based on a 'complete' Riemann solver with all waves in the solution of the Riemann problem leads to much more accurate results whereas the cost of the scheme rises only by 10%, see [28, 27] for the evaluation of fluxes in WENO/MPWENO schemes. For the WAF and ADER-WAF schemes we find it helpful, but not crucial, to use characteristic projection as given by (39) - (41) for problems involving strong shocks. However for the kind of test problems as those presented here we find that there is no visible difference in the results obtained with and without characteristic projection. For ADER, ADER-WAF, WENO and MPWENO schemes the finite-volume WENO reconstruction is carried out in characteristic variables.

Example 3. Modified shock/turbulence interaction.

We use a test problem that is a variation of the shock/turbulence problem proposed in [7, 1]. We solve the Euler equations (14) on $[-5, 5]$ with initial condition

$$(\rho, u, p) = \begin{cases} (1.515695, 0.523346, 1.80500), & x < -4.5 \\ (1 + 0.1 \sin 20\pi x, 0.0, 1.), & x > -4.5 \end{cases} \tag{46}$$

which consists of a right facing shock wave of Mach number 1.1 running into a high-frequency density perturbation. As the shock moves into this perturbation it spreads

upstream. The solution contains physical oscillations which have to be resolved by the numerical method. It is for such type of problems when sophisticated higher order schemes should give better results than lower order ones.

We compute the flow at the output time $t = 5$ which is more than ten times larger than that of the standard shock/turbulence problem [1]. For the calculations shown here we choose a coarse mesh of 1000 cells so that there are only four-five cells between each extrema in the physical oscillations. Again we use CFL=0.95 for WAF, WENO5, ADER and ADER-WAF schemes and CFL=0.3 for the MPWENO9 scheme. Note that since the shock wave is weak here it might be possible to run the MPWENO scheme with higher CFL numbers; however, to be consistent we still use the CFL number which is required by the monotonicity constraint. Results are shown in Figs. 11 - 19. In all figures symbols denote the numerical solution and the solid line denotes the reference solution, computed using the ADER5-WAF scheme on a mesh of 5000 cells.

All calculations have been run on a personal computer with Athlon-XP 1700+ processer (1.533 Ghz clock frequency). We use Compaq Visual Fortran Compiler 6.0 with full optimisation to generate the corresponding code. Computing times are given for the whole run on the given mesh for each scheme used with its corresponding CFL number.

Figs. 11 and 12 show that on the mesh of 1000 cells the WAF and WENO5 schemes severely damp the acoustic disturbance which spreads upstream of the shock. The result confirms the observation in [43] that for such meshes with very few cells per wave length the WENO5 scheme quickly loses accuracy. The MPWENO9 scheme (Fig. 13) again is much more accurate than WENO5. It is interesting to see that this problem is more sensitive to the spatial discretisation than to the formal order of accuracy; on a similar problem the MPWENO9 scheme outperforms WENO5 scheme although both schemes use the third order ODE solver [1].

The accuracy of the original ADER schemes (Figs. 14-16) improves as we go from the third order to the fifth order scheme. ADER3 is slightly more accurate for this problem than WENO5 (Fig. 12) but still the resolution is very poor due to the same reason as for the WENO5 scheme. Forth and fifth order ADER schemes are more accurate. However, we see that the ADER5 scheme is slightly less accurate than the MPWENO9 scheme for this problem.

Finally, we observe that new ADER-WAF schemes of this paper (Figs. 17-19) are far superior to the corresponding original ADER schemes (Figs. 14-16). The difference in accuracy is evident for schemes of all orders. Clearly, the ADER4-WAF achieves the same accuracy as the MPWENO9 scheme does and outperforms the ADER5 scheme (Fig. 16). The ADER5-WAF (Fig. 19) is the most accurate scheme for this problem.

When comparing computing times of the WENO5, MPWENO9 and ADER-WAF schemes we see that the ADER-WAF schemes are the fastest schemes. There are two major reasons for this. Firstly, the ADER-WAF schemes are one-step schemes whereas WENO/MPWENO schemes use the three stage Runge-Kutta method for time discretisation. Procedures such as data reconstruction, characteristic decomposition, evaluation of nonlinear WENO weights, back projections and evaluation of the flux must be done at each stage. Of course, the ADER-WAF schemes have the additional expense of solving the linearised Riemann problems for spatial derivatives and performing the Cauchy-Kowalewski procedure. However, all linearised Riemann problems have the same matrix $\mathbf{A}^{(0)}_{i+1/2}$, this greatly reduces the cost of solving the derivative Riemann problems. Secondly, the range of CFL numbers that a given scheme can use in practical computations must also be a

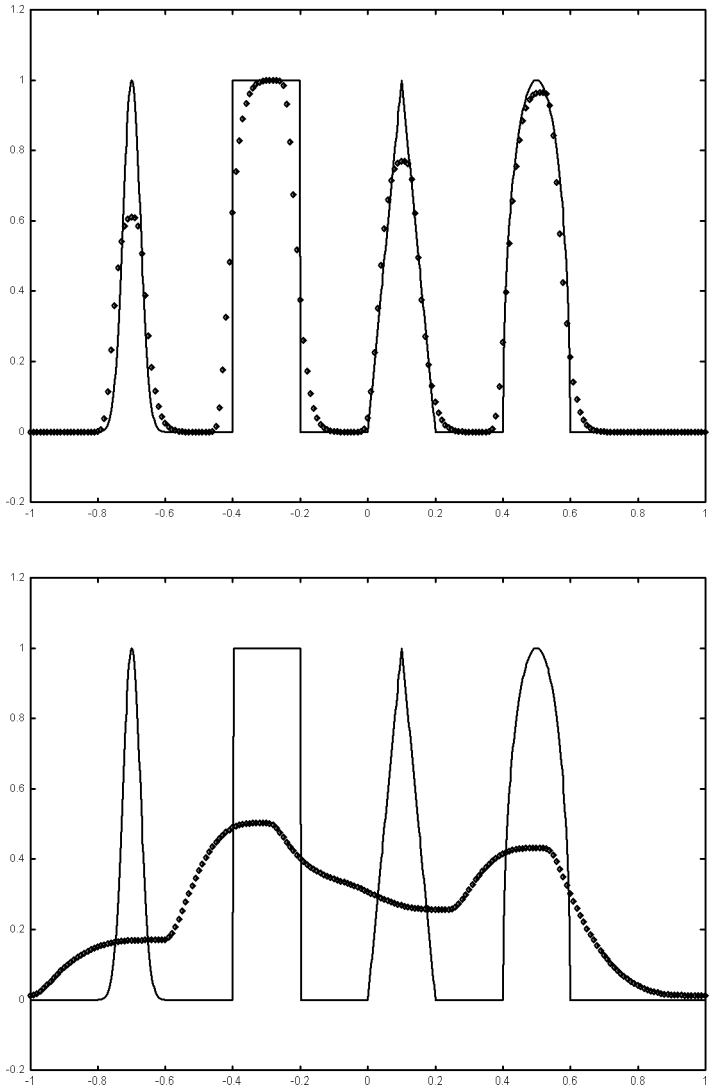

Figure 1: Computed (symbol) and exact (line) solutions for the linear advection equation (42) with initial condition (45) at output times $t = 20$ (top) and $t = 2000$ (bottom). Method used: WAF with van Leer limiter, CFL=0.95 and N=200 cells

factor in discussing efficiency. The ADER-WAF schemes use much higher CFL numbers than WENO/MPWENO schemes; namely 0.95 versus 0.3 for the MPWENO9 scheme. All these factors result in the observed difference in speed, shown in the legends of Figs. 12-19. In two space dimensions, finite-difference schemes are in general expected to be faster than finite-volume schemes. However, the difference should be smaller for ADER and ADER-WAF schemes than for WENO schemes, because the former are one-step schemes and can use higher CFL numbers.

We note that the test problem for the Euler equations contains a rather weak shock and therefore the test does not assess the robustness of the schemes for strong shock waves. We remark however that we have successfully solved the complete suit of very demanding test problems proposed by Toro [31] and the blast wave interaction problem of Woodward and Colella [44] using ADER-WAF schemes of this paper; results are omitted.

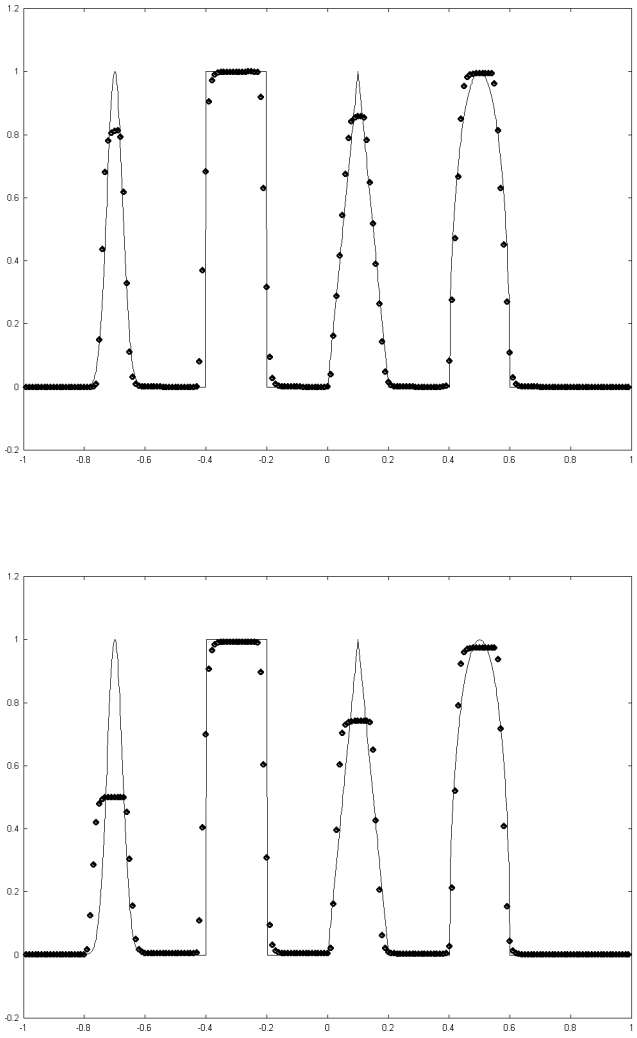

Figure 2: Computed (symbol) and exact (line) solutions for the linear advection equation (42) with initial condition (45) at output times $t = 20$ (top) and $t = 2000$ (bottom). Method used: WAF with SUPERBEE limiter, CFL=0.95 and N=200 cells

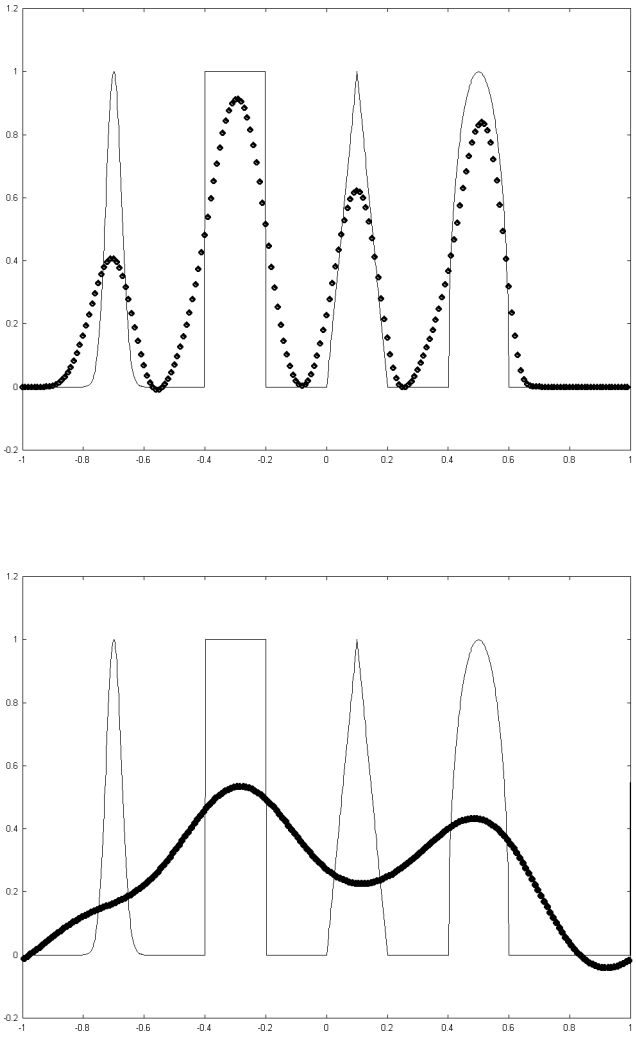

Figure 3: Computed (symbol) and exact (line) solutions for the linear advection equation (42) with initial condition (45) at output times $t = 20$ (top) and $t = 2000$ (bottom). Method used: WENO5, CFL=0.95 and N=200 cells

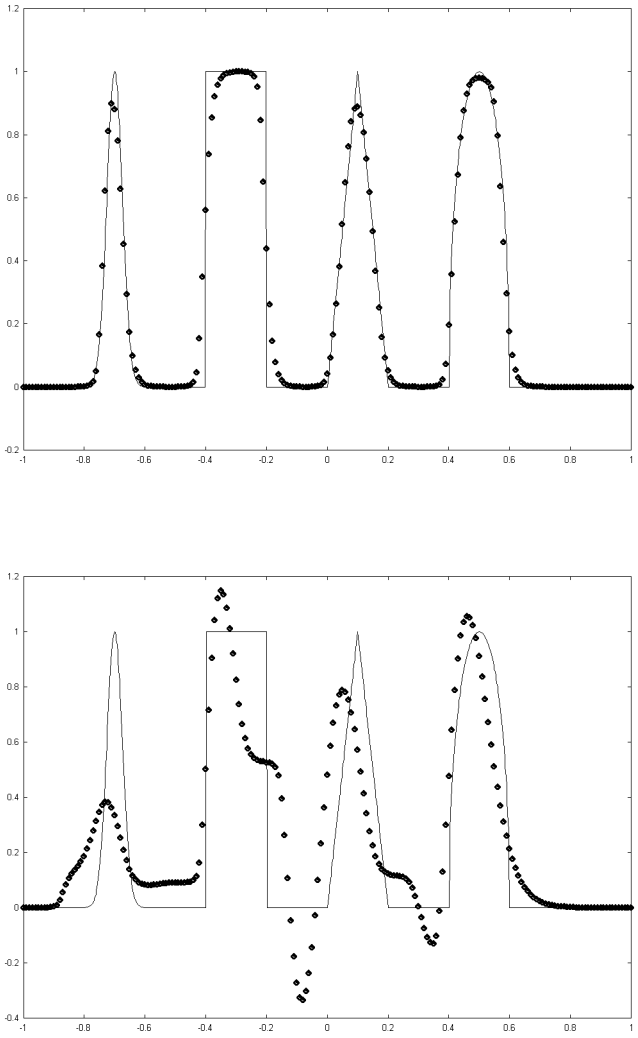

Figure 4: Computed (symbol) and exact (line) solutions for the linear advection equation (42) with initial condition (45) at output times $t = 20$ (top) and $t = 2000$ (bottom). Method used: ADER3, CFL=0.95 and N=200 cells

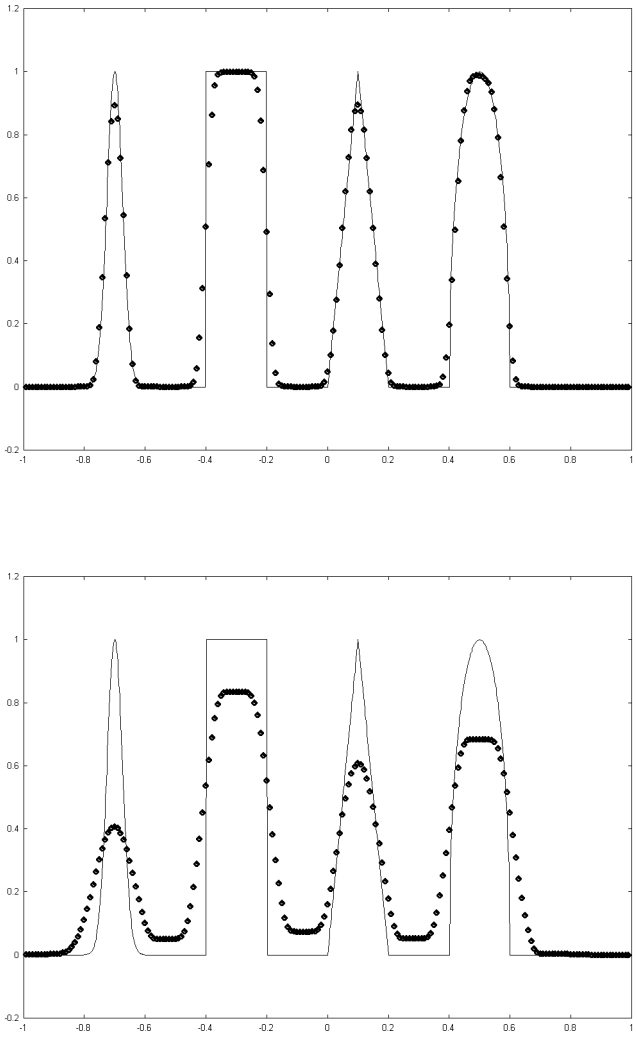

Figure 5: Computed (symbol) and exact (line) solutions for the linear advection equation (42) with initial condition (45) at output times $t = 20$ (top) and $t = 2000$ (bottom). Method used: MPWENO9, CFL=0.3 and N=200 cells

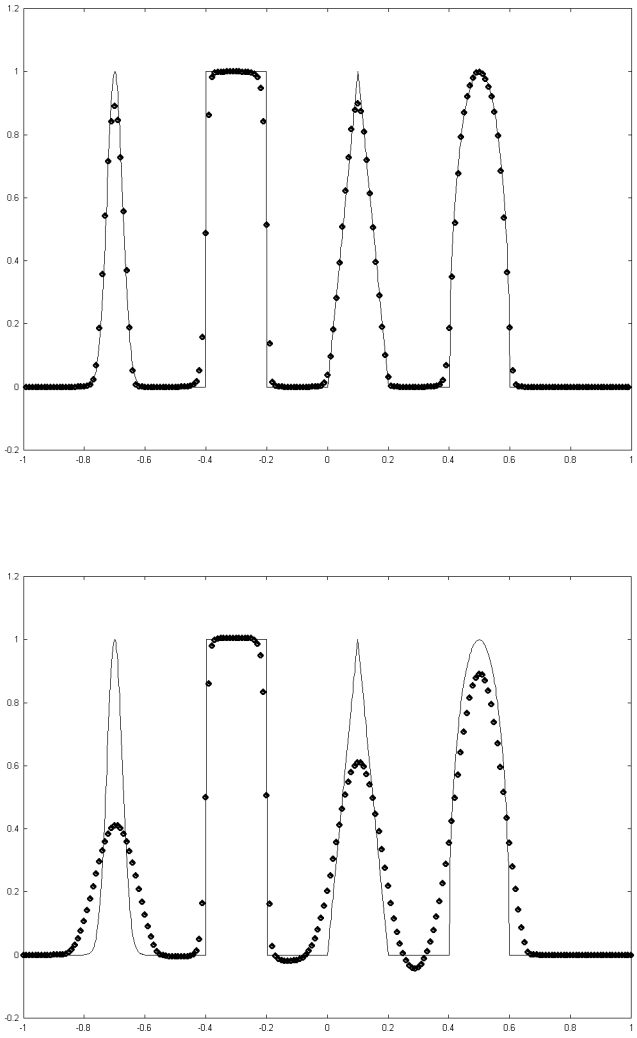

Figure 6: Computed (symbol) and exact (line) solutions for the linear advection equation (42) with initial condition (45) at output times $t = 20$ (top) and $t = 2000$ (bottom). Method used: ADER3-WAF, CFL=0.95 and N=200 cells

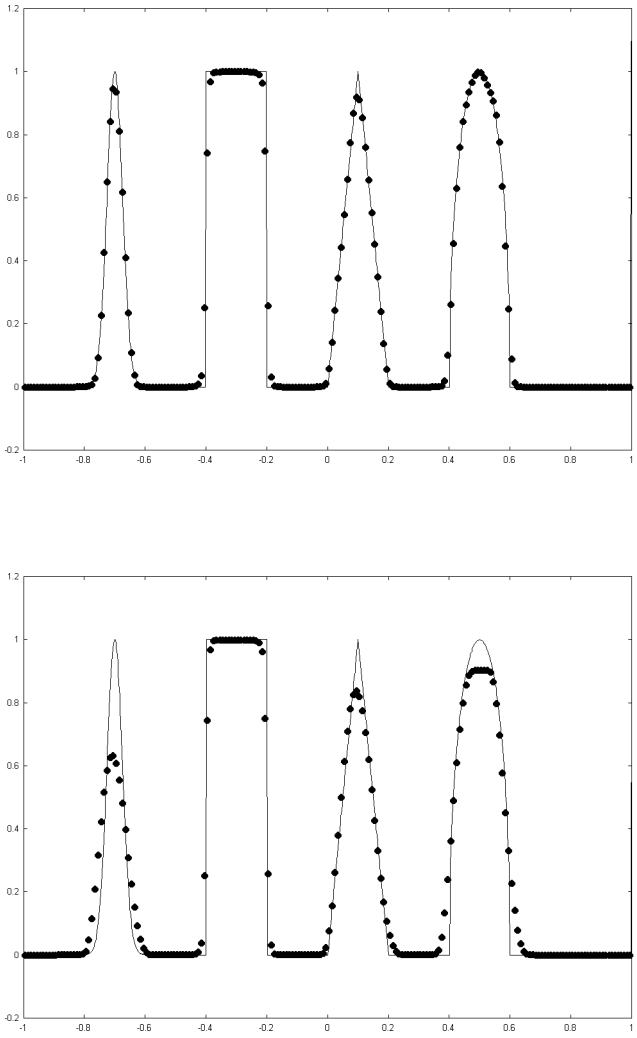

Figure 7: Computed (symbol) and exact (line) solutions for the linear advection equation (42) with initial condition (45) at output times $t = 20$ (top) and $t = 2000$ (bottom). Method used: ADER4-WAF, CFL=0.95 and N=200 cells

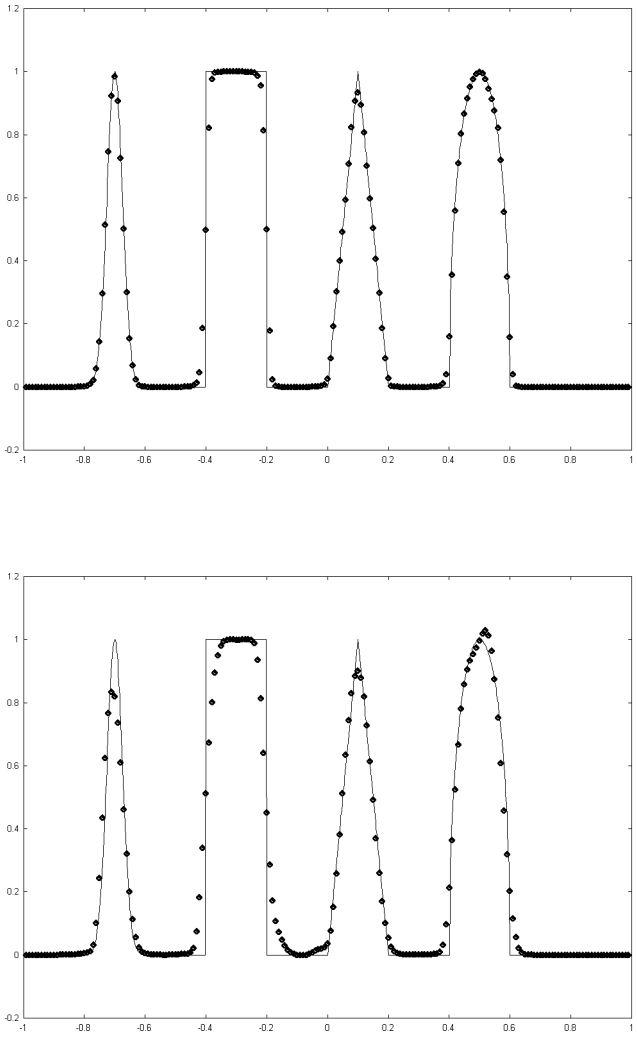

Figure 8: Computed (symbol) and exact (line) solutions for the linear advection equation (42) with initial condition (45) at output times $t = 20$ (top) and $t = 2000$ (bottom). Method used: ADER5-WAF, CFL=0.95 and N=200 cells

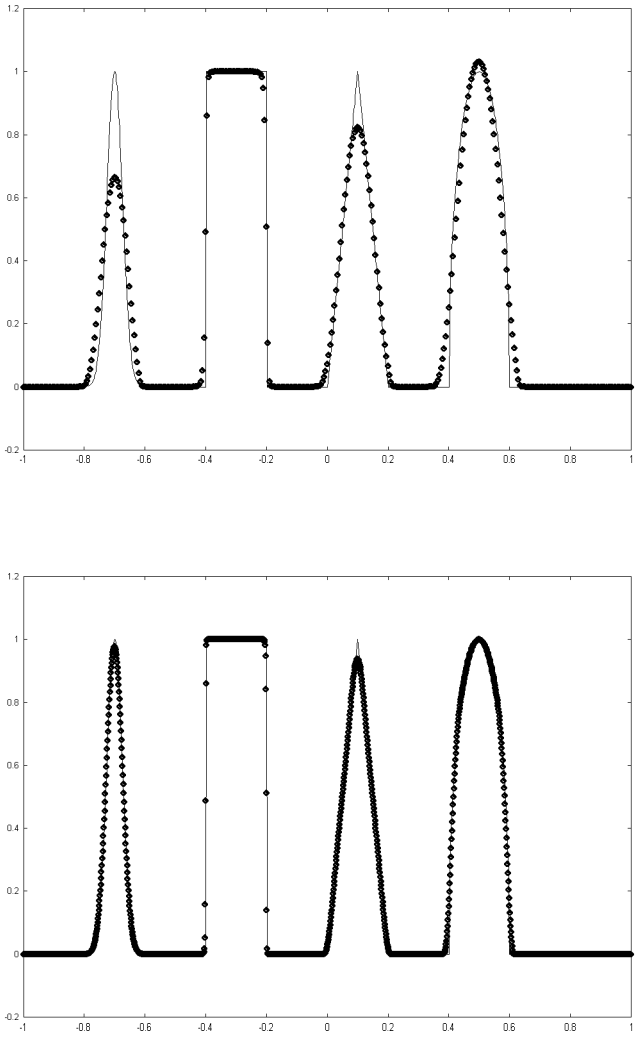

Figure 9: Computed (symbol) and exact (line) solutions for the linear advection equation (42) with initial condition (45) at output time $t = 2000$. Method used: ADER3-WAF, CFL=0.95, N=400 cells (top) and N=1600 cells (bottom)

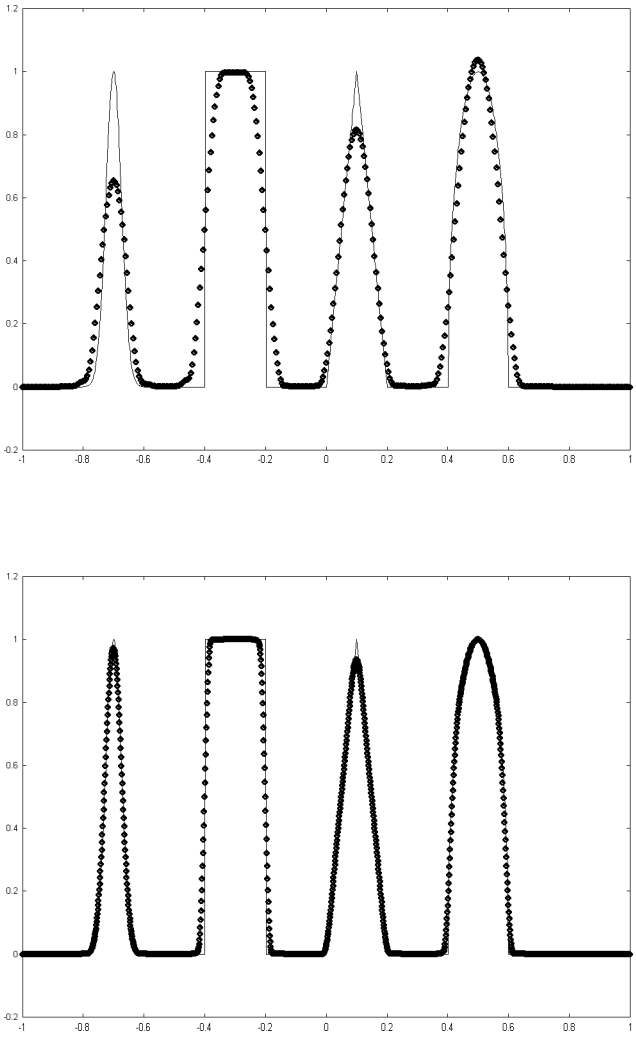

Figure 10: Computed (symbol) and exact (line) solutions for the linear advection equation (42) with initial condition (45) at output time $t = 2000$. Method used: MPWENO9, CFL=0.3, N=400 cells (top) and N=1600 cells (bottom)

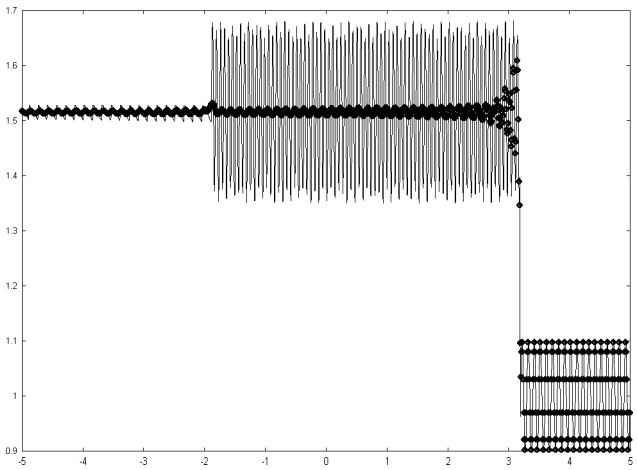

Figure 11: Computed (symbol) and reference (line) solutions for the Euler equations (14) with initial condition (46) at output time $t = 5$. Method used: WAF, CFL=0.95 and N=1000 cells. Computing time 1.5s

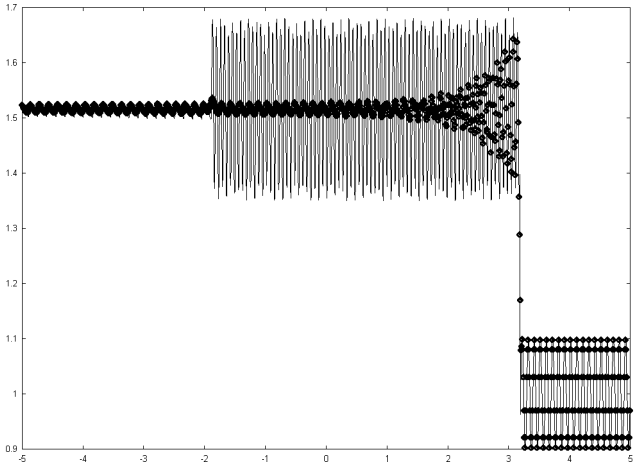

Figure 12: Computed (symbol) and reference (line) solutions for the Euler equations (14) with initial condition (46) at output time $t = 5$. Method used: WENO5, CFL=0.95 and N=1000 cells. Computing time 6s.

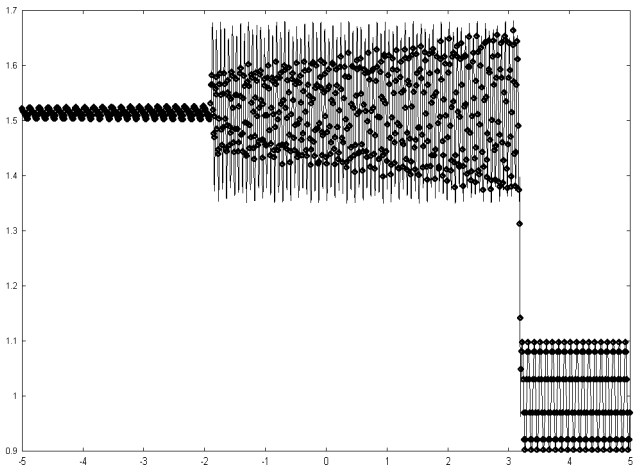

Figure 13: Computed (symbol) and reference (line) solutions for the Euler equations (14) with initial condition (46) at output time $t = 5$. Method used: MPWENO9, CFL=0.3 and N=1000 cells. Computing time 48s

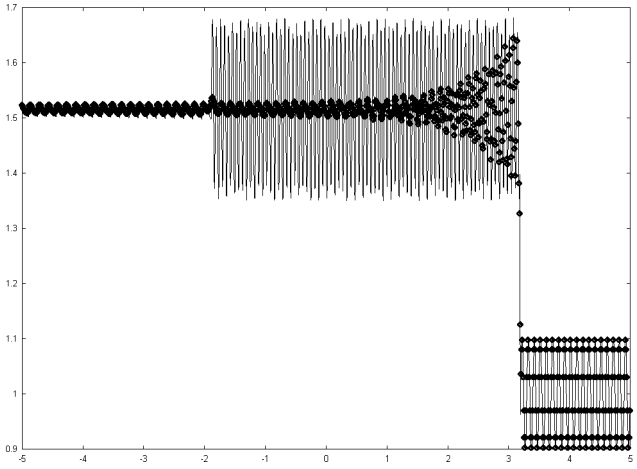

Figure 14: Computed (symbol) and reference (line) solutions for the Euler equations (14) with initial condition (46) at output time $t = 5$. Method used: ADER3, CFL=0.95 and N=1000 cells. Computing time 2.5s.

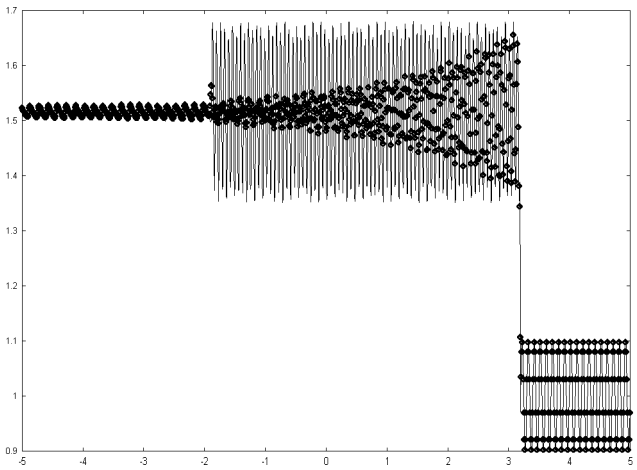

Figure 15: Computed (symbol) and reference (line) solutions for the Euler equations (14) with initial condition (46) at output time $t = 5$. Method used: ADER4, CFL=0.95 and N=1000 cells. Computing time 6.5s.

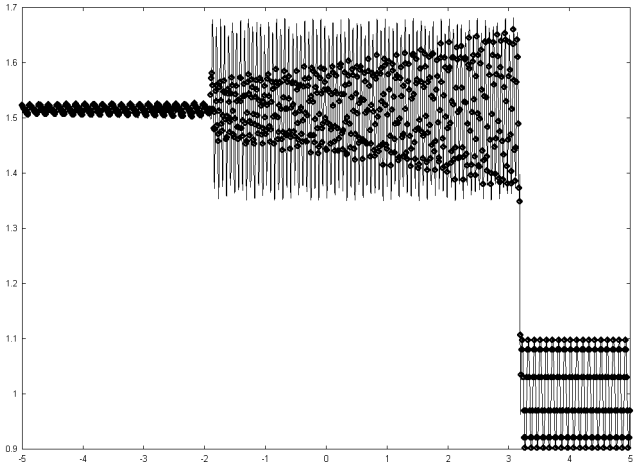

Figure 16: Computed (symbol) and reference (line) solutions for the Euler equations (14) with initial condition (46) at output time $t = 5$. Method used: ADER5, CFL=0.95 and N=1000 cells. Computing time 11s.

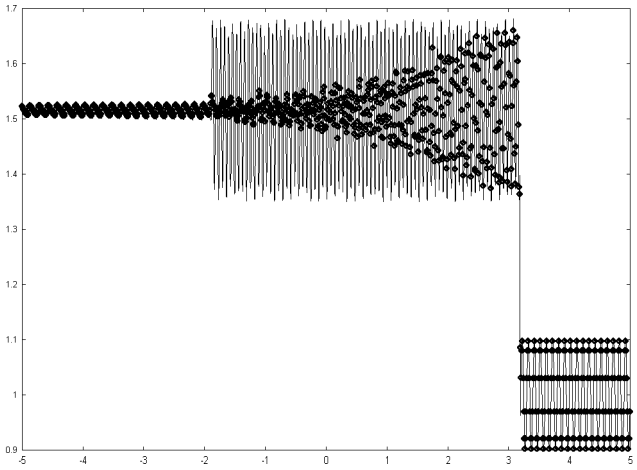

Figure 17: Computed (symbol) and reference (line) solutions for the Euler equations (14) with initial condition (46) at output time $t = 5$. Methods used: ADER3-WAF and N=1000 cells. Computing time 6.5s

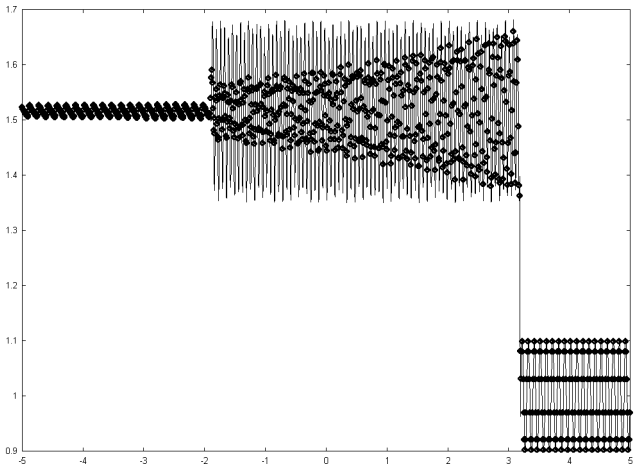

Figure 18: Computed (symbol) and reference (line) solutions for the Euler equations (14) with initial condition (46) at output time $t = 5$. Methods used: ADER4-WAF and N=1000 cells. Computing time 9.5s.

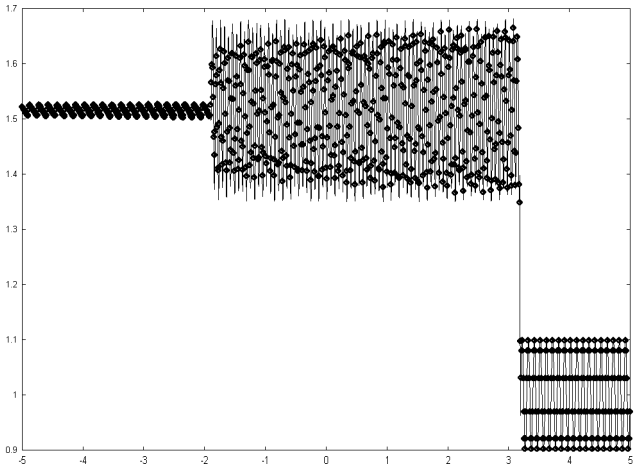

Figure 19: Computed (symbol) and reference (line) solutions for the Euler equations (14) with initial condition (46) at output time $t = 5$. Method used: ADER5-WAF, CFL=0.95 and N=1000 cells. Computing time 15s.

7. Summary and future developments

In this paper we have first developed a new variant of the ADER approach based on a flux expansion rather than a state expansion, as originally proposed in the ADER approach. This variant makes it possible to use the full range of monotone first-order fluxes available, and which are conventionally used as the building block for schemes of high-order of accuracy. The second contribution of this paper concerns the proposition of using a TVD flux, rather than a first-order monotone flux, as the building block. We show that such TVD flux results in very substantial improvements to the accuracy of the schemes and of their convergence rates. The improvements are most evident for problems involving very long-time evolution, which are the kind of problems that fully justifies the development of sophisticated schemes.

We systematically compare the numerical results of the schemes presented in this paper with those obtained from other schemes, such as TVD methods, the original ADER schemes, WENO and MPWENO schemes. The numerical experiments suggest that the schemes of this paper are superior to all others by a clear margin.

Future developments will include extension of the ADER-WAF methods to non-linear multidimensional problems, based on the successful preliminary results for two-dimensional linear problems [35, 21], and application of the ideas of this paper to ENO, WENO and MPWENO schemes and Runge-Kutta Discontinuous Galerkin methods of [4]. We will consider not only upwind TVD fluxes but also centred TVD fluxes. See [27] for centred and upwind ENO-TVD, WENO-TVD and MPWENO-TVD schemes applied to one-dimensional Euler equations.

References

[1] Balsara D. S. and Shu C.W. (2000). Monotonicity preserving weighted essentially non-oscillatory schemes with increasingly high order of accuracy. *J. Comp. Phys.*,

160, pp. 405-452.

[2] Batten P., Clarke N., Lambert C. and Causon D.M. (1997). On the choice of wave speeds for the HLLC Riemann solver. *SIAM J. Sci. Stat. Comput.*, **18**(6), pp. 1553-1570

[3] Ben-Artzi M. and Falcovitz J. (1984). A second-Order Godunov-type scheme for compressible fluid dynamics. *J. Comp. Phys.*, **55**, pp. 1-32.

[4] Cockburn B. and Shu C.-W. (2001). Runge-Kutta Discontinuous Galerkin methods for convection-dominated problems. *J. Sci. Comput.*, **16** , pp. 173-261.

[5] Godunov S. K. (1959). A finite difference method for the computation of discontinious solutions of the equation of fluid dynamics. *Mat. Sb.*, **47**, pp. 357-393.

[6] Gurski K.F. (2002). An HLLC approximate Riemann solver for ideal magnetohydrodynamics, submitted for publication.

[7] Jiang G.S. and Shu C.W. (1996). Efficient implementation of weighted ENO schemes. *J. Comput. Phys.*, **126**, pp. 202-212.

[8] Harten A. (1983). High Resolution Schemes for Hyperbolic Conservation Laws. *J.Comp. Phys.*, **49**, pp. 357-393.

[9] Harten A., Engquist B., Osher S. and Chakravarthy S.R. (1987). Uniformly high order accurate essentially non-oscillatory schemes III. *J. Comput. Phys.*, **71** , pp. 231-303.

[10] Harten A. , Lax P. D., and van Leer B. (1983). On upstream differencing and Godunov-type schemes for hyperbolic conservation laws. *SIAM Review* **25**(1), pp. 35 - 61.

[11] Kolgan N.E. (1972). Application of the minimum-derivative principle in the construction of finite-difference schemes for numerical analysis of discontinuous solutions in gas dynamics. *Uchenye Zapiski TsaGI* [Sci. Notes of Central Inst. of Aerodynamics], **3**, No. 6, pp. 68-77 (in Russian).

[12] Kolgan N.E. (1975). Finite-difference schemes for computation of two dimensional discontinuous solutions of nonstationary gas dynamics. *Uchenye Zapiski TsaGI* [Sci. Notes of Central Inst. of Aerodynamics], **6**, No. 1, pp. 9-14 (in Russian).

[13] Kolgan N.E. (1975). Finite-difference schemes for computation of three dimensional solutions of gas dynamics and calculation of a flow over a body under an angle of attack. *Uchenye Zapiski TsaGI* [Sci. Notes of Central Inst. of Aerodynamics], **6**, No. 2, pp. 1-6 (in Russian).

[14] R.J. LeVeque Numerical Methods for Conservation Laws. Birkhauser Verlag, 1992.

[15] Liu X.D. and Osher S. and Chan T. (1994). Weighted essentially non-oscillatory schemes. *J. Comput. Phys.*, **115** pp. 200-212.

[16] Men'shov I.S., (1991). Generalized problem of break-up of a single discontinuity. *Prikl. Matem. i Mekhan.*, **55**, No. 1, pp.86-95 (*Journal of Applied Mathematics and Mechanics*).

[17] Men'shov I.S., (1990). Increasing the order of approximation of Godunov's scheme using solution of the generalized Riemann problem. *U.S.S.R. Comput. Math. Phys.*, **30**, No. 5, pp.54-65.

[18] Men'shov I.S., (1992). Accuracy increase of the Godunov scheme for stationary supersonic Euler equations based on the solution of generalized Riemann problem. *U.S.S.R. Comput. Math. and Math. Phys.*, **32**, No. 2, pp.257-263.

[19] Roe P.L. (1985). Some contributions to the modelling of discontinuous flows. *Lect. Appl. Math.*, **22**.

[20] Rusanov V.V. (1961). Calculation of interaction of non-steady shock waves with obstacles. *J. Comp. Math. Phys., USSR*, **1**, pp. 267-279.

[21] Schwartzkopff T., Munz C.D., Toro E.F. and Millington R.C. (2002). ADER-2D: a high-order approach for linear hyperbolic systems in 2D. *J. Sci. Comput.*, **17**, pp. 231-240.

[22] Suresh A. and Huynh T. (1997). Accurate monotonicity preseving scheme with Runge-Kutta time stepping. *J. Comput. Phys*, **136**, pp. 83-99.

[23] Sweby P.K. (1984). High resolution schemes using flux limiters for hyperbolic conservation laws. *SIAM J. Numer. Anal.*,**21**, pp 995-1011.

[24] Takakura Y. and Toro E.F. (2002). Arbitrarily accurate non-oscillatory schemes for a nonlinear conservation law. *Computational Fluid Dynamics Journal*, **11**, No. 1, pp. 7-18.

[25] Titarev V.A. (2001). *Very High Order ADER Schemes for Nonlinear Conservation Laws*. Department of Computing and Mathematics, Manchester Metropolitan University, UK, MSc. Thesis.

[26] Titarev V.A. and Toro E.F. (2002). ADER: Arbitrary High Order Godunov Approach. *J. Sci. Comput.*, **17**, pp. 609-618.

[27] Titarev V.A. and Toro E.F. (2002). On the use of TVD flluxes in ENO and WENO schemes, submitted.

[28] Titarev V.A. and Toro E.F. Assessment of first order fluxes in high order finite-volume WENO and MPWENO schemes, in preparation.

[29] Titarev V.A. and Toro E.F. (2003). High order ADER schemes for advection-diiffusion-reaction equations *CDF Journal*, to appear

[30] Toro E.F. *Some aspects of shock capturing methods for gas dynamics*. CoA report 9112, August 1991, Department of Aerospace Science, Cranfield Institute of Technology.

[31] Toro E.F. (1999). *Riemann Solvers and Numerical Methods for Fluid Dynamics.* Second Edition, Springer-Verlag.

[32] Toro E.F. (1998). Primitive, conservative and adaptive schemes for hyperbolic conservation laws. In: *Numerical Methods for Wave Propagation*, pp 323-385. E F Toro and J F Clarke (editors). Kluwer Academic Publishers.

[33] Toro E.F. (1989). A weighted average flux method for hyperbolic conservation laws. *Proceedings of the Royal Society of London*, A 423, pp 401-418.

[34] Toro E.F. (1992). The weighted average flux method applied to the Euler equations. *Phil. Trans. of the Royal Society of London*, A 341, pp 499-530.

[35] Toro E.F., Millington R. C. and Nejad L. A. M. (2001). Towards very high order Godunov schemes. In:*Godunov Methods. Theory and Applications*, Edited Review, E. F. Toro (Editor), Kluwer/Plenum Academic Publishers, pp 907-940.

[36] Toro E.F., Spruce M. and Speares W. (1994). Restoration of the Contact Surface in the Harten-Lax-van Leer Riemann Solver. CoA report 9204, January 1992, Dapertment of Aerospace Science, Cranfield Institute of Technology.

[37] Toro E.F., Spruce M. and Speares W. (1994). Restoration of the contact surface in the Harten-Lax-van Leer Riemann solver. *Journal of Shock Waves*, **4**, pp. 25-34.

[38] Toro E.F. and Titarev V. A. (2002). Solution of the Generalised Riemann Problem for Advection-Reaction Equations. *Proc. Roy. Soc. London*, **458**, N2018, pp. 271-281.

[39] Toro E.F. and Titarev V.A. (2001). Very high order Godunov-type schemes for nonlinear scalar conservation laws. In *European Congress on Computational Methods in Applied Sciences and Engineering ECCOMAS Computational Fluid Dynamics Conference 2001, Swansea, Wales, UK, 4-7 September, 2001.*

[40] Toro E.F. and Titarev V.A. (2001). The ADER approach for nonlinear advection-diffusion-reaction equations. In: *The 8th National Conference on Computational Fluid Dynamics*, E-Land, Taiwan, August 18-20, 2001.

[41] van Leer B. (1973). Towards the ultimate conservative difference scheme I: the quest for monotonicity. *Lecture Notes in Physics* **18**, pp. 163-168.

[42] van Leer B. (1979). Towards the ultimate conservative difference scheme V: a second order sequel to Godunov' method. *J. Comput. Phys.* **32**, pp. 101-136.

[43] Wang Z. J. and Chen R. F. (2001). Optimized weighted essentially non-oscillatory schemes for linear waves with discontinuity. *J. Comp. Phys.*, **174**, No. 1, pp. 381-404.

[44] Woodward P. and Colella P. (1984). The numerical simulation of two-dimensional fluid flow with strong shocks. *J. Comp. Phys.*, **54**, pp. 115-173.